The design of a small water tunnel and its use in evaluating surface roughness effects on cavitation

Kaku, Ken
Laboratory of science and engineering of soil, Department of Agriculture, Kyushu University

https://doi.org/10.5109/22734

出版情報：九州大学大学院農学研究院紀要. 13 (3), pp.527-584, 1965-05. Kyushu University
バージョン：
権利関係：

Journal of the Faculty of Agriculture, Kyushu University, Vol. 13, No. 3,
‘May 30, 1965

The design of a small water tunnel and its use in evaluating surface roughness effects on cavitation

Ken **KAKU**

I. INTRODUCTION

Outline of cavitation phenomenon

If a significant pressure reduction takes place at a point in water flow, a cavity would appear at the point. The cavity will flow downstream with the flowing water and will suddenly disappear at a higher pressure region. The appearance and disappearance of the cavity will continue to occur successively as long as the low pressure exists. This phenomenon is known as cavitation.

Previous investigations have suggested that the value of the limiting pressure at which cavitation usually commences is not zero absolute, but somewhat higher, i.e. the so-called vapor pressure at which water begins to vaporize. The mechanism of it is that, if the local pressure at the point drops to the vapor pressure, vapor bubbles will form and expand suddenly by vaporization of water through the bubble walls. This is the commonly accepted concept of cavitation. However, there is another mechanism of cavitation as described below. The amount of dissolved gas in water will affect the value of the limiting pressure. The more dissolved gas which is contained in water, the easier it diffuses from water and forms gas bubbles if the pressure is low enough. The gas bubbles will expand relatively slowly by diffusion of gas through the bubble walls. This phenomenon, also, has to be included in cavitation. To avoid confusion, the former cavitation is called vaporous cavitation and the latter is called gaseous cavitation. The limiting pressure value for gaseous cavitation is higher than that for vaporous cavitation.

For these reasons, it can only be said that there will be a possibility of forming cavitation at the point where the local pressure is

lowered to a limiting value which is nearly equal to the vapor pressure of water at the bulk temperature.

When the static pressure at a point in flowing water drops to the limiting pressure value, tiny vapor bubbles or gas bubbles will form. The bubbles grow to a certain size due to vaporization or diffusion, then they will be collapsed by the surrounding water as they are carried downstream into a higher pressure region. This process of bubble formation, growth and collapse occurs in rapid succession. The impact force of collapse is so great that, if cavitation occurs near a boundary surface, it sometimes results in erosion or pitting on the surface. Pitting is the most disadvantageous result of cavitation on a hydraulic structure, for it could cause the destruction of the whole structure. In addition, its efficiency will be reduced by the disturbance of flow and vibration resulting from cavitation. Therefore, one of the more important problems in the design of a hydraulic structure is the prediction of the onset of cavitation.

For a submerged body, the below equation is obtained from Bernoulli's equation.

$$\frac{V_0^2}{2g} + \frac{P_0}{\gamma} = \frac{V^2}{2g} + \frac{P}{\gamma} \qquad (1)$$

where V_0 and P_0 are the free stream velocity and the free stream static pressure respectively, V and P are the local velocity and the local static pressure at a point on the boundary surface, γ is the specific weight of water. The above equation will be changed as

$$\frac{P_0 - P}{1/2\rho \cdot V_0^2} = \left(\frac{V}{V_0}\right)^2 - 1 \qquad (2)$$

where p is the mass density of water.

The left hand side of Eq. (2) is commonly called the pressure coefficient for the body and expressed as

$$C_p = \frac{P_0 - P}{1/2\rho \cdot V_0^2} \qquad (3)$$

As obviously known from Eq. (2) the pressure coefficient has the minimum value of -1 at the stagnation point of the body and has the maximum value at the minimum pressure point. The maximum value is called the minimum pressure coefficient for the body which is expressed as

$$C_{p\,\min} = \frac{P_0 - P_{\min}}{1/2\rho \cdot V_0^2} \qquad (4)$$

where $C_{p\,\min}$ is the minimum pressure coefficient.

A water flow condition in connection with cavitation is usually indicated by the factor σ which is called cavitation number.

$$\sigma = \frac{P_0 - P_v}{1/2\rho \cdot V_0^2} \tag{5}$$

where σ is the cavitation number and P_v is the vapor pressure of water at the bulk temperature. The cavitation number at the onset of cavitation will, then, be expressed as

$$\sigma_i = \frac{P_i - P_v}{1/2\rho \cdot V_0^2} \tag{6}$$

where σ_i is the cavitation number at the onset of cavitation and P_i is the free stream static pressure at the onset of cavitation.

Comparing Eq. (4) and (6), it may be true to state that the cavitation number at the onset of cavitation is equal to the minimum pressure coefficient for the body, because P_v will first appear at the minimum pressure point. Therefore, as long as the cavitation number for a body in a flow condition is smaller than the minimum pressure coefficient for the body, cavitation will not occur on the body. Once σ becomes larger than $C_{p\,\min}$, cavitation takes place on the body.

Cavitation can be obtained in laboratories by either changing the free stream static pressure while keeping the free stream velocity constant, or changing the free stream velocity while keeping the free stream static pressure constant. At any rate, one will observe two regimes of flow as changing the condition, i.e. non-cavitating flow and cavitating flow. Between the two regimes there is a stage of limited cavitation where a very small number of cavitation bubbles is in existence. The limited cavitation will be achieved by changing the flow condition from both sides, i.e. decreasing the free stream static pressure from the non-cavitating flow regime or increasing it from the cavitating flow regime, while keeping the free stream velocity constant. The limiting pressure values for these two procedures are usually not same. The difference is called cavitation hysteresis. Holl[12] defined the limited cavitation achieved by decreasing the static pressure as incipient cavitation and one achieved by increasing the static pressure as desinent cavitation. Cavitation numbers which correspond to the incipient cavitation and desinent cavitation are called incipient cavitation number and desinent cavitation number respectively. In equation forms

$$\sigma_i = \frac{P_i - P_v}{1/2\rho \cdot V_0^2} \tag{7}$$

$$\sigma_d = \frac{P_d - P_v}{1/2\rho \cdot V_0^2} \qquad (8)$$

where σ_i is the incipient cavitation number and σ_d is the desinent cavitation number, P_i and P_d are limiting pressures correspond to incipient and desinent cavitation respectively. Previous investigations have shown that the incipient cavitation occurs randomly while the desinent cavitation is rather stable and repeatable, and that the former is equal to or smaller than the latter. Many experimental investigations of cavitation have been conducted in the way to determine the desinent cavitation number, because of the repeatability and because it could be considered as the safe side. However, the incipient cavitation number may be more an important factor for an actual cavitation than the desinent cavitation number.

Cavitation scale effects

Although many workers have investigated cavitation phenomenon, the true mechanism of it has not been unveiled yet. Therefore, the exact similarity law of cavitation has not been established yet. Furthermore, the similarity law of cavitation illustrated below is extremely difficult to satisfy. Neverthless, it may be valuable to discuss the basic requirements of cavitation similarity and to keep them in ones mind while he investigates cavitation.

1. The classical theory of similarity

It has been accepted as the theory of similarity for cavitation that, for geometrically similar flow systems, the ratio of the difference in static pressure between two points to the free stream velocity pressure is a constant as long as the liquid is nonviscous and incompressible. It is expressed as follows.

$$\frac{P}{1/2\rho \cdot V_0^2} = \text{constant} \qquad (9)$$

P: the difference in static pressure between two points

$1/2\rho \cdot V_0^2$: the free steam velocity pressure

For the condition of the onset of cavitation, Eq. (9) will be expressed as

$$\sigma_i = \frac{P_i - P_v}{1/2\rho \cdot V_0} = \text{constant} \qquad (10)$$

σ_i: the cavitation number for the onset of cavitation

P_i: the limiting pressure

P_v: the vapor pressure of water at the bulk temperature

Eq. (10) states that onsets of cavitation on geometrically similar bodies take place at the same cavitation number. In other word, an experiment concerning the investigation of cavitation can be done equally by using geometrically similar bodies.

Although the classical theory of similarity had surved well, recent investigations have shown that cavitation did not follow the theory. It is not surprising, if one considers the basic assumption of the classical theory of similarity. The assumption will be stated as follows :

a. Pressure differences in the flow are caused by free stream velocity pressure, i.e. the fluid is assumed to be incompressible and frictionless.

b. The pressure at which cavitation starts is the vapor pressure of the liquid and the value is constant for the particular flow field.

c. There is no tention in the liquid and there are no time effects, so that cavitation starts instantaneously whenever the vapor pressure is reached.

Furthermore, the assumption of geometric similarity includes that of surface roughness.

2. Scale effects of cavitation

For an actual flow, the assumption stated above can not be applied and, therefore, there will be some departures in cavitation condition from the classical theory of similarity. This departure has been termed as " scale effects of cavitation." To avoid confusion, scale effects are usually divided into two groups and discussed separately as

a. scale effects on the minimum pressure in the liquid.

b. scale effects on the cavitation pressure and on the growth of cavitation voids.

a. Scale effects on the minimum pressure in the liquid

To gain a similar flow condition in an actual flow to an ideal flow, it is known that the similarity laws of Reynolds, Froude and Mach should be satisfied, i.e.

$$R = \frac{V \cdot L}{\mu \cdot \rho} = \text{constant} \quad \text{(Reynolds number)}$$

$$F = \frac{V}{\sqrt{g \cdot L}} = \text{constant} \quad \text{(Froude number)}$$

$$M = \frac{V}{a} = \text{constant} \quad \text{(March Number)},$$

a: the velocity of propagation of a pressure wave within the flow field

For a liquid, the value of μ/ρ and a are constant, so that $V \cdot L$, V/L and V should be kept constant which is impossible. None of these numbers can be neglected in cavitation flow[13], so that the departure is inevitable.

Another factor which affects the minimum pressure is surface roughness. It can be neglected, if the surface is sufficiently smooth, but actually the surface is rough. Although surface roughness is to be included in the geometric similarity, it is practically impossible to reform similar surface roughness on the surface. The surface roughness, if the relative height of which is large, could cause a significant reduction of the local pressure. Therefore, the minimum pressure would be lowered at the point from that which would be predicted for a smooth surface. Namely, cavitation on a rough surface will occur at a larger minimum pressure coefficient than that which is predicted for a smooth surface.

b. Scale effects on the cavitation pressure and on the growth of cavitation voids

Since vapor pressure of a liquid changes with temperature, the change in local temperature resulting from the process of vaporization through cavity walls should be considered. Pleasset and Zwick[22] investigated the problem theoretically and found that, although the change in temperature is small, the effect is appreciable. This was confirmed by Dergaradedian.[3] Holl and Wislicenus[13] stated that the heat transfer would be expressed as

$$\Delta T = \text{constant} \cdot \frac{a_v}{a_l} \cdot \frac{V_l}{V_v} \cdot \frac{\lambda}{C_{pl}} \cdot P_e^n \qquad (11)$$

where $0 < n < 1$ and,

a_v area of vapor removal through the liquid

a_l : area of heat supply through the liquid

V_l : specific volume of the liquid

V_v : specific volume of the vapor

λ latent heat of vaporization

C_{pl} : the specific heat of the liquid

P_e : $= \frac{C_{pl}}{V_l \cdot K} \cdot V \cdot L$, K is the coefficient of heat conduction

and vapor pressure reduction is

$$\Delta P_v = \frac{\partial P_v}{\partial T} \cdot \Delta T \qquad (12)$$

The condition of similarity is

$$\frac{\Delta P_v}{P} = \text{const.} \tag{13}$$

where P is a representative, absolute, pressure in the system.

It has been established theoretically by using fracture theory that, if there are no initial voids in water, through the walls of which vaporization occurs and which grow to cavities, a tension of the order of thousands of atmospheric pressure is required to have a separated cut in water? Water subjected to negative pressure is in a metastable state and vapor bubbles are observed to grow from small nuclei. Application of nucleation theory considering the above fact estimated the fracture pressure of the order of hundreds of atmospheric pressure.[4] However, tensions are not applied in usual cavitation experiments using water. The only reasonable explanation of the fact is the existence of cavitation nuclei with diameters ranging from 10^{-5} to 10^{-3} cm. These nuclei will act as weak points and grow to cavities at the point in water where the pressure is sufficiently low to cause vaporization of water or diffusion of gas from water. There are still some difficulties concerning the presence and existence of the nuclei. It has been shown that the rate of gas solution by diffusion is so large that gas bubbles will dissolve very rapidly in under-saturated solution, for example, an air bubble of radius 10^{-3} will dissolve in saturated water in about 8 sec., and faster in under-saturated water.[25] Furthermore, a bubble will tend to rise to free surface and also disappear there. Thus, there must be some mechanism to prevent the solution or disappearance of nuclei. Harvey") suggested that nuclei would exist in water as trapped gas pockets on crevices of boundary surface. The water can not dissolve the gas, because the gas pressure is less than the water pressure by the effect of surface tension. Fox and Herzfeld[5] assumed that an organic skin formed from contaminants in water surrounds the bubble and acts as a rigid sphere.

Gilmore and Plesset[7] established the similarity law for cavitation concerning surface tension and cavitation nuclei as follows

$$\frac{\rho \cdot V^2 \cdot L}{\sigma_s} = \text{const.} \tag{14}$$

σ_s: surface tension

$$\frac{A}{L} = \text{const.} \tag{15}$$

A: size of nuclei

$$n = N \cdot L^3 = \text{const.} \tag{16}$$

n: the number of cavitation nuclei in the flow

N: the number of cavitation nuclei per unit volume of the fluid

Cavitation damages

1. The mechanism

Possible harmful effects of cavitation on a hydraulic structure are the surface erosion which is sometimes called pitting, the reduction in efficiency and the vibration in the structure or in the water flow. Among these effects, the most undesirable one is the surface erosion, for it may cause destruction of the whole structure. The mechanism of the surface erosion has not been clarified yet, but the most well accepted reasoning of it is that the erosion is the mechanical damage caused by the local stress developed in the liquid when cavitation bubbles collapse there. The damage could be accelerated by the erosive action of chemical and electrochemical effects.“”) The value of the maximum pressure developed by the collapse of a cavitation bubble can not be predicted, because the mechanism of the bubble behavior is yet unknown. However, from experience, it can be stated that the collapse pressure is high enough to cause mechanical damages on a material surface. Jones[14] measured the pressure in an experiment using deaerated water and stated that it is at least 12,000 atm. and it occurs in a time of order of microsecond.

2. Examples of damages on hydraulic structures

Hydraulic structures are mostly made of concrete, and the surface of concrete is usually rough so that cavitation occurs relatively easily. Furthermore, concrete is more likely to be suffered from cavitation damage than metals, because of the concrete property. Recently, the cavitation damage on the concrete surface has become an important problem in the field of Hydraulic Engineering, as the designs of hydraulic structures have become larger and therefore surfaces become likely to expose to higher water speed.

There have been several examples of damages on concrete surface of hydraulic structures. Harrold[8] reported that the cavitation erosion of the concrete surface in the spillway of Bonneville Dam on the Columbia River was observed. Hickox[10] reported heavy damages in the sluices of Norris Dam on the Tenesse River. Colgate”) reported the cavitation damage at Davis Dam on the Colorado River. He mentioned that the initial erosion was caused by cavitation and then the erosion was accelerated by the jet action of high speed water flow.

The author and others investigated the spillway surface of Kamishiiba Dam on the Mimi-Kawa. The Kamishiiba Dam is an arch Dam having a hight of 110 meters and was constructed in 1955.[16] Two

spillways were installed at both sides of the Dam to discharge the maximum discharge of 1,800 m^3/sec. Water discharged through tainter gates, installed above the spillway, falls down 40 meters along the spillway and jumps into air at the down-stream end of it as Fig. 1.

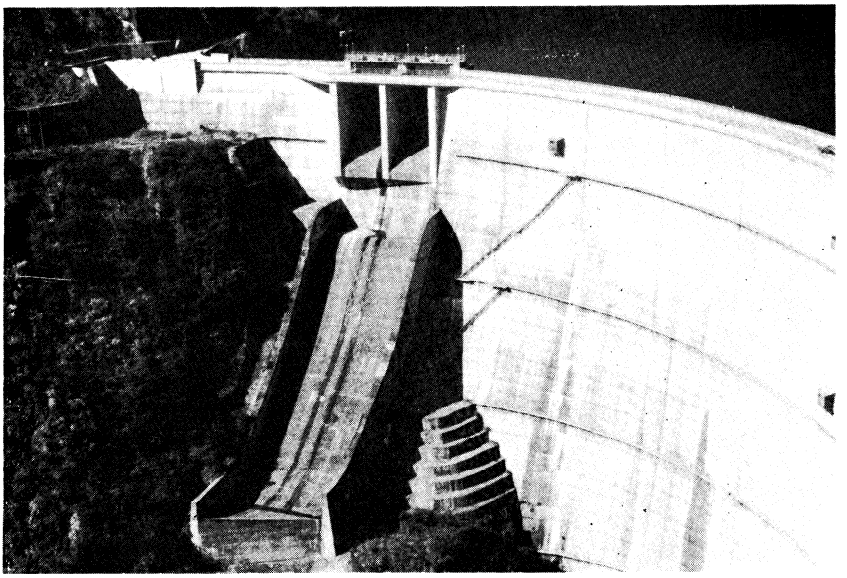

Fig. 1. Kamishiiba dam spillway.

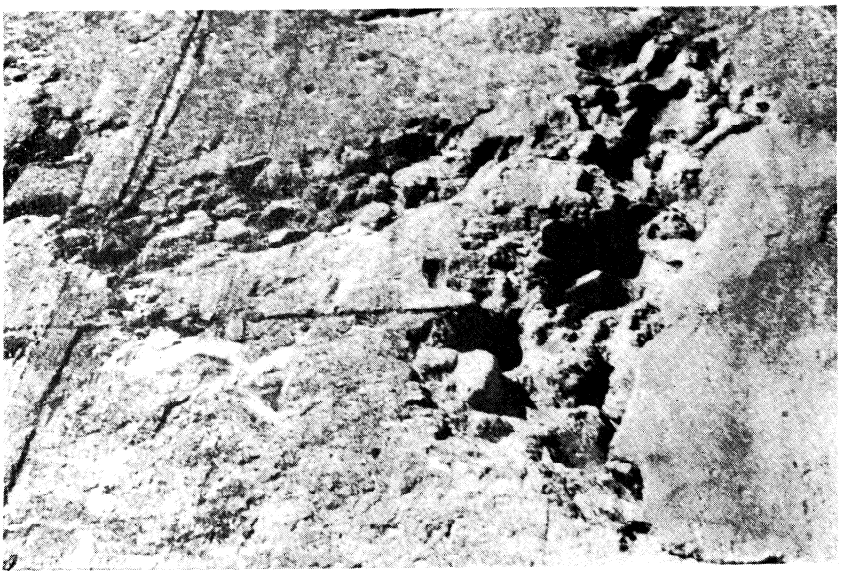

Fig. 2. Eroded concrete surface.

The width of the spillway is 20.8 meters at the upstream end and 18.8 meters at the downstream end. Figs. 2-4 show typical eroded surfaces. The erosion becomes heavier at the downstream part than the upstream

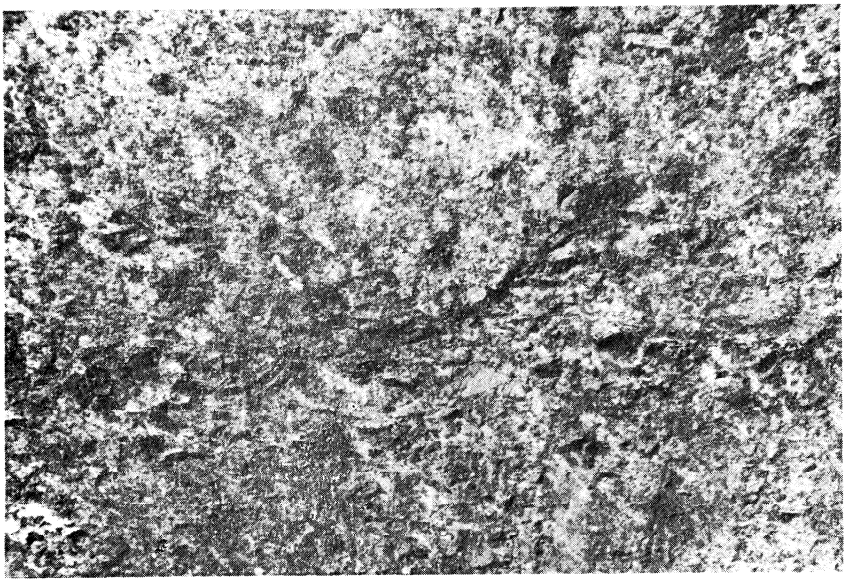

Fig. 3. Eroded concrete surface.

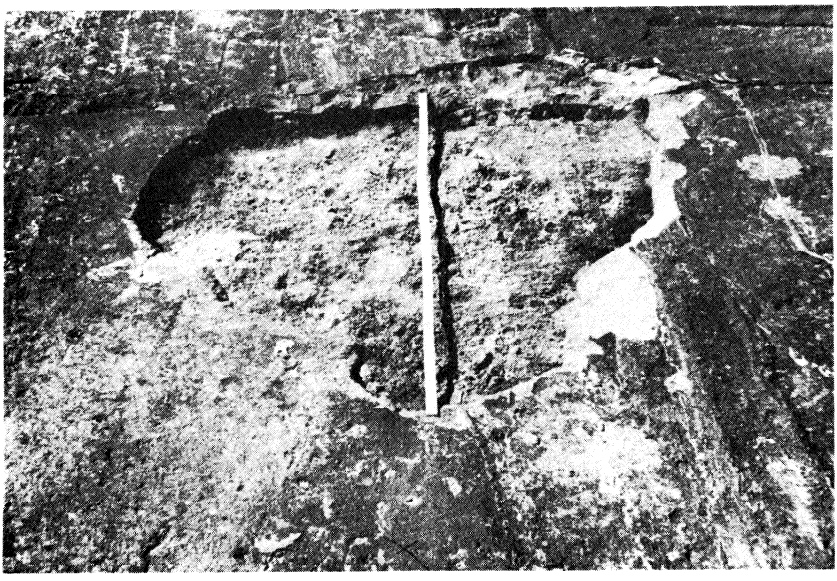

Fig. 4. Eroded concrete surface.

part. It would be caused by the increase of velocity at the part. Another significance was that the part of concrete joint was eroded severely, even if it existed at relatively upstream. At the downstream part of a small hole was also eroded significantly. It was probably caused by the local pressure reduction at sharp edges of the hole. At some points, the erosion grew to a big hole as Fig. 4. It could be caused by jet action of high velocity water flow.

Method of investigating the cavitation phenomenon

1. Water tunnel

For the experimental investigation of cavitation, one of the more desirable items of equipment is a water tunnel as then the experiment can be conducted under a wide range of free stream velocities and free stream static pressure. Furthermore, the observation window, usually installed at the middle of the upper part of the tunnel, enables one to observe cavitation visually and acoustically.

Water tunnels are usually classified into two types, circulating and noncirculating types. With the noncirculating water tunnel, there is no problem of the occurrence of noise which could be caused by the pump. This would interfere the acoustic measurements. Although the control of velocity and pressure in the working section is relatively easy in a circulating type, the noise generated by the pump or impeller will be carried by the water and the tunnel walls to the working section, so that acoustic measurements become difficult. An important factor in cavitation experiments is the control of the free stream velocity and the free stream static pressure. Therefore, if the noise problem is solved, it is better to use a circulating water tunnel. Constructions of circulating type water tunnels in recent years have shown the possibility of designing a circulating water tunnel which produces only low noise levels, thus permitting acoustic measurements.

There are two choices of the type of working section in a circulating type water tunnel, i.e. an open jet or a closed jet. The former is convenient for tests of short models such as propellers, because the diameter of working section is relatively large compared to the length of it. The latter is convenient for tests of elongated models such as torpedoes, because of the relatively long working section. For example, the 20 inch water tunnel at the Massachusetts Institute of Technology is an open jet circulating type water tunnel and is used for tests of propellers, while the 14 inch water tunnel at the California Institute of Technology is a closed jet circulating type and is used for tests of elongated models (Figs. 5 and 6). For tests of propellers, the existence of the propeller shaft sometimes makes it

necessary to bring the shaft through the shell as shown in Fig. 5. Bringing out the shaft requires the first turn to be near the working section, resulting in poor flow conditions. The 48 inch water tunnel

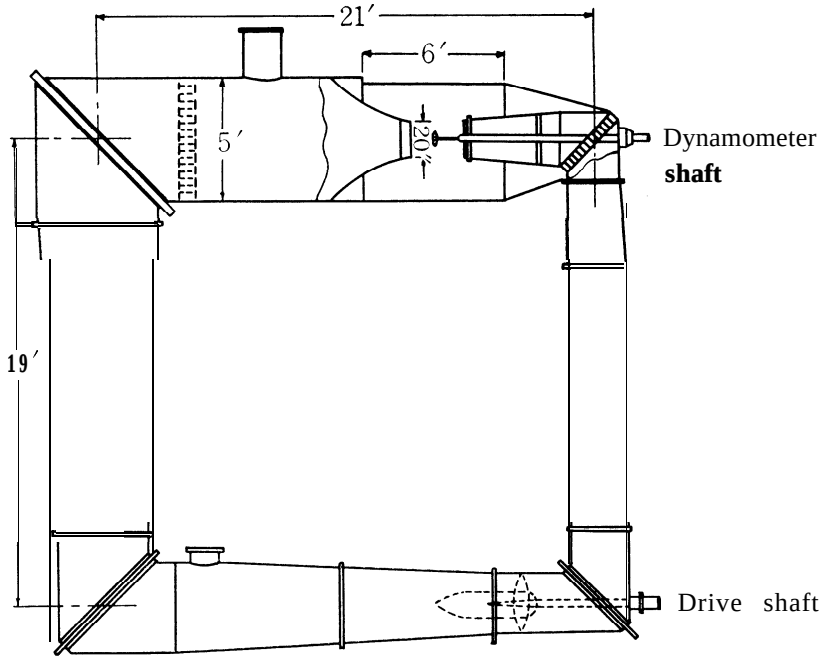

Fig. 5. Twenty inch water tunnel at the Mass. Institute of Technology.

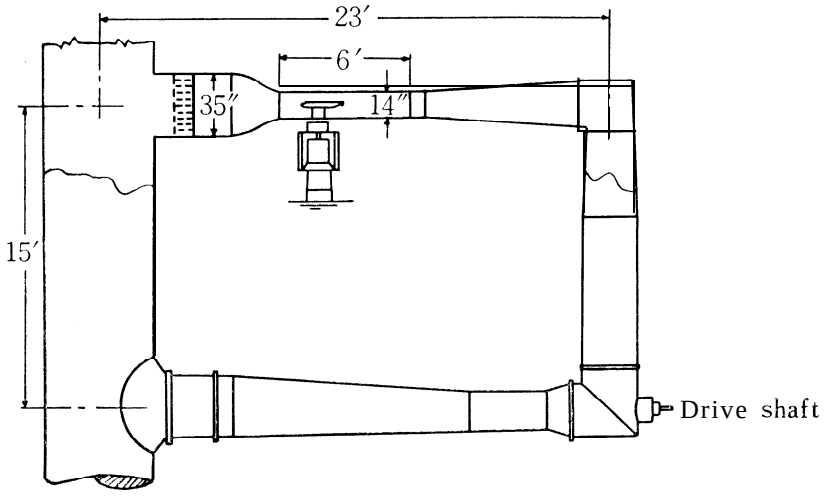

Fig. 6. Fourteen inch water tunnel at the California Institute of Technology.

at the Ordnance Research Laboratory of the Pennsylvania State University solved the problem by installing motors in the models themselves. This water tunnel is a closed jet circulating type water tunnel and is used for tests of propellers behind torpedo models (Fig. 7).

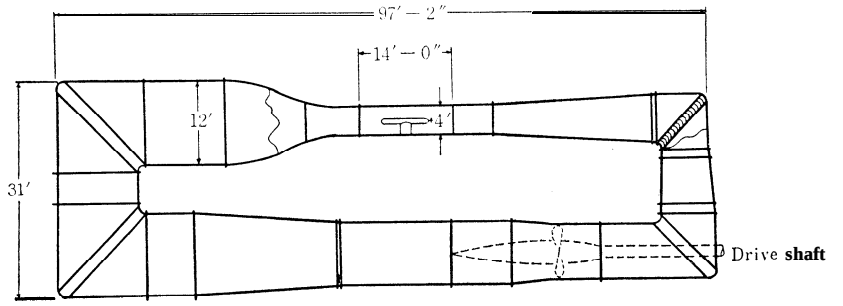

Fig. 7. Forty eight inch water tunnel at the Ordnance Research Laboratory of Pennsylvania State University.

2. Closed circuit vacuum tank

Although a water tunnel is a convenient equipment for the investigation of cavitation, a model test of a hydraulic structure having free surface, for example a dam, can not be undertaken. To

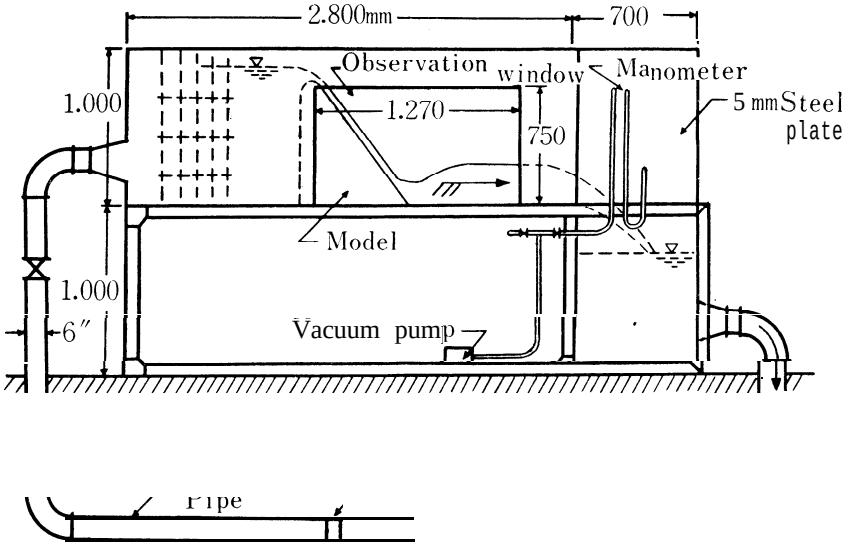

Fig. 8. Closed circuit vacuum tank.

undertake model tests of such structures and observe directly the points and shapes of cavitation, a closed circuit vacuum tank is used successfully. It consists of a vacuum tank with an observation window and a water circulating system.

Tanabe and others[20] designed a closed circuit vacuum tank as Fig. 8 and constructed it at the Hydraulic Laboratory of Irrigation Engineering, Faculty of Agriculture, Kyushu University. The similarity relation of a model is as follows. To conduct a model test of L_r scale, the air pressure in the vacuum tank has to be kept as

$$P_{am} = L_r \cdot P_{ap} + (1 - L_r) P_v \tag{17}$$

where P_{am} is the air pressure in the tank, P_{ap} is the atmospheric pressure for the prototype and P_v is the vapor pressure of water at the bulk temperature.

3. Other equipments

To investigate pitting damages on material surfaces from cavitation, it is sometimes desirable to accelerate the rate of pitting. Pitting is known to be produced at a higher rate by high frequency pressure variation than by ordinary cavitation. High frequency acceleration of the test specimen relative to the liquid produces a high frequency pressure variation and heavier pitting on the specimen. This acceleration is obtained by the application of the magnetostrictive effect on a nickelrod to the end of which the test specimen is attached as Fig. 9.[21] Plesset and Ellis[23] developed a method for generating the pressure variations by exciting a resonance in the water cavity. The equipment is not a suitable device to investigate cavitation characteristics, for the cavitation developed in it is not a true cavitation. Neverthless, if one's desire is directed only to the investigation of cavitation damages, the equipment could be a most convenient one. Cavitation damages can be obtained in a short period and the cost of construction is relatively low.

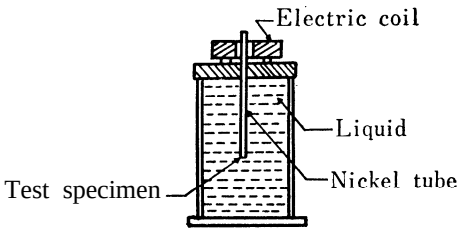

Fig. 9. Apparatus for producing cavitation by vibratory method.

II. Surface roughness effects on cavitation

Because of harmful effects of cavitation, the design of a cavitation

free structure or the prediction of the onset of cavitation on the structure is an important problem for a hydraulic engineer. It can be done relatively easily by a theoretical analysis or a model experiment, if the surface of the structure is smooth. However, the surface of an ordinary structure is rough. The roughness may be scattered randomly as concrete surfaces or may be isolated as poor matings of component materials. Therefore, there will be some departure between the predicted condition and the actual condition, being affected by scale effects of surface roughness on cavitation.

The major scale effect

According to the classical theory of similarity, the cavitation number for a body at the onset of cavitation σ_i is equal to the minimum pressure coefficient $C_{p\min}$ for the body. Thus,

$$\sigma_i = C_{p\ \min} \tag{18}$$

If surface roughness, randomly distributed or isolated, exists on the body, it may cause the local pressure reduction at the minimum pressure point. Then, the minimum pressure coefficient $C_{p\min R}$ will increase from that for the smooth body. Therefore,

$$C_{p\min R} > C_{p\min} \tag{19}$$

A cavitation free hydraulic structure is to be designed under the condition that the cavitation number for the body σ is

$$\sigma > \sigma_i \tag{20}$$

If $C_{p\min R}$ is large enough, the below condition could be reached from above relations

$$\sigma < C_{p\min R} \tag{21}$$

In this condition, cavitation may occur on the body. The above simple analysis shows that surface roughness could cause cavitation to occur on a structure at the designed condition.

The minimum pressure coefficient for a body with roughness $C_{p\min R}$ will be expressed as

$$C_{p\ \min\ R} = \frac{P_i - P_{\min R}}{1/2\rho \cdot V_0^2} \tag{22}$$

where $P_{\min R}$ is the minimum pressure on the body, P_i is the free stream static pressure and V_0 is the free stream velocity. Eq. (22) may be written as

$$C_{p\min R} = \frac{P_i - P}{1/2\rho \cdot V_0} + \frac{P - P_{\min}}{1/2\rho \cdot V^2}\left(\frac{V}{V_0}\right)^2 \tag{23}$$

Letting P and V be the static pressure and velocity at the minimum pressure point on the body without roughness, the below equation will

be followed.

$$\left(\frac{V}{V_0}\right)^2 = \frac{1/2\rho\cdot V^2}{1/2\rho\cdot V_0^2} = \frac{1/2\rho\cdot V_0^2+P_i-P}{1/2\rho\cdot V_0} = 1 + C_{p\,\min} \qquad (24)$$

Assume that the roughness consists of an irregularity having a minimum pressure coefficient Of $C_{p\,\min 0}$ when it is on a flat plate, then

$$C_{p\,\min 0} = \frac{P-P_{\min R}}{1/2\rho\cdot V^2} \qquad (25)$$

Substituting Eq. (24) and (25) to Eq. (23), the below equation is followed,

$$C_{p\,\min R} = C_{p\,\min} + (1+C_{p\,\min})\cdot C_{p\,\min 0} \qquad (26)$$

If cavitation occurs when the minimum pressure is equal to vapor pressure at the bulk temperature, then from Eq. (26)

$$\sigma_R = \sigma_i + (1+\sigma_i)\,\sigma_{i0} \qquad (27)$$

where σ_R is the cavitation number for the body with roughness, σ_{i0} is the cavitation number for the irregularity when it is on a flat plate and σ_i is the cavitation number for the body without the irregularity. Therefore, the cavitation number for a body with roughness could be predicted by knowing the minimum pressure coefficient for the body without roughness and the cavitation number for the roughness.

Minor scale effect

Kermeen[15] investigated the effect of surface finish on cavitation by testing two hemispheres (two inches in diameter), one of which was made of glass and another was made of stainless steel. The surface of the stainless steel was first finished with hand to a bright lustre, then was roughened by sand blasting and finally was painted to a smooth surface. He found that the desinent cavitation number for the roughened model was smaller than that for smooth surfaces. The result is shown in Fig. 10. The reason could be that the mean surface pressure on the rough surface was increased by thickening the boundary layer and consequently the minimum pressure coefficient was decreased. Therefore the desinent cavitation number is decreased. As shown in the above example, surface roughness may cause the desinent cavitation number to decrease, if the height of the roughness is not high enough to reduce the local pressure.

Holl[12] suggested the existence of the spots of cavitation. Finding the desinent cavitation number, one may observe the spots of cavitation remaining on the boundary surface after the uniformly distributed cavitation disappeared. The desinent cavitation number for the spots of cavitation is much higher than that expected. He concluded that the spots of cavitation was gaseous cavitation. Air bubbles of the

gaseous cavitation probably be stabilized by being trapped by the surface roughness or be stabilized on the surface in the adverse pressure gradient following the minimum pressure point. Thus, the surface roughness may cause a considerable increase of the desinent cavitation number.

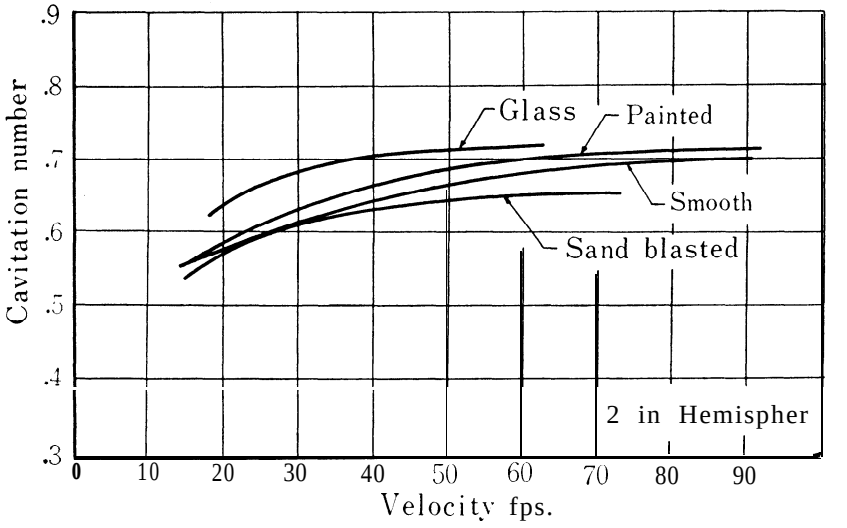

Fig. 10. Effect of model surface finish on cavitation number at maximum acoustic pressure for 2 inch diameter hemispheres.

Minimum pressure coefficient for a semi circular irregularity

It is extremely difficult to investigate theoretically the effects of randomly distributed surface roughness, for there has not been any systematical work on the problem and the boundary layer characteristic of a rough surface has not been known. The most simplified form of randomly distributed surface roughness could be considered as an isolated surface irregularity. To simplify the problem further, one may assume that the irregularity has an two dimentional semicircular profile and exists on a flat plate.

1. Potential flow on a semicircular irregularity

The complex potential for a uniform stream with a uniform velocity of U_∞ in the c-plane parallel to the real axis is

$$W = U_\infty \cdot \zeta \tag{28}$$

Assuming that there is an infinitely thin plate SH having a width of 4a in the C-plane as Fig. 11, the uniform stream is mapped into the flow around a circular cylinder of radius a in the Z-plane by the

transformation[17]

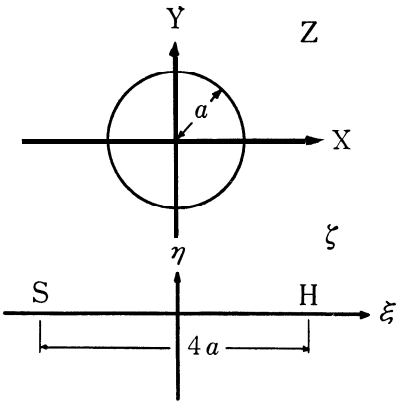

Fig. Il. Transformation, $\eta = Z + \frac{a^2}{Z}$.

$$\zeta = Z + \frac{a^2}{Z} \qquad (29)$$

Thus, the complex potential of the flow past the cylinder is

$$W = U_\infty \left(Z + \frac{a^2}{Z} \right) \quad (30)$$

Letting ϕ and ψ be the potential function and the stream function respectively

$$w = \phi + i\psi \qquad (31)$$

Therefore, the stream function is

$$\psi = U_\infty \cdot Y \left(1 - \frac{a^2}{X^2 + Y^2} \right) \quad (32)$$

The speed of the potential flow q is expressed by

$$q^2 = \frac{dW}{dZ} \cdot \frac{d\overline{W}}{dZ} \qquad (33)$$

On the cylinder

$$q^2 = 4U^2_\infty \cdot \sin^2\theta \qquad (34)$$

The minimum pressure $P_{\min}$ occurs on the cylinder at $\theta = 90°$. Thus denoting the free stream pressure as P_∞, and applying Bernoulli's equation, the below equation will be obtained

$$P_{\min} + 2\rho \cdot U^2_\infty = P_\infty + 1/2\, \rho \cdot U^2_\infty \qquad (35)$$

The minimum pressure coefficient for the body, $C_{p\,\min\infty}$, then be

$$\mathbf{C}_{p\,\min\infty} = \frac{P_\infty - P_{\min}}{1/2\rho \cdot U^2_\infty} = 3 \qquad (36)$$

The pressure distribution on a two dimentional semicircular irregularity existing on a flat plate is the same as that on the circular cylinder. Therefore, the onset cavitation number for the irregularity is

$$\sigma_i = 3 \qquad (37)$$

2. Application of the frozen streamline theory

An isolated surface irregularity having a semicircular profile is assumed to exist on a flat plate and be imbeded in a boundary layer having a thickness of 6, at a far upstream point as Fig. 12. The X axis coincides with the boundary surface and has zero point at the

center of the irregularity. Symbols Y, δ, V, U are the distance from the surface, the boundary layer thickness, the velocity outside the boundary layer and the velocity inside the boundary layer. The subscript infinity (∞) denotes conditions X = $-\infty$ and zero (0) at X = 0.

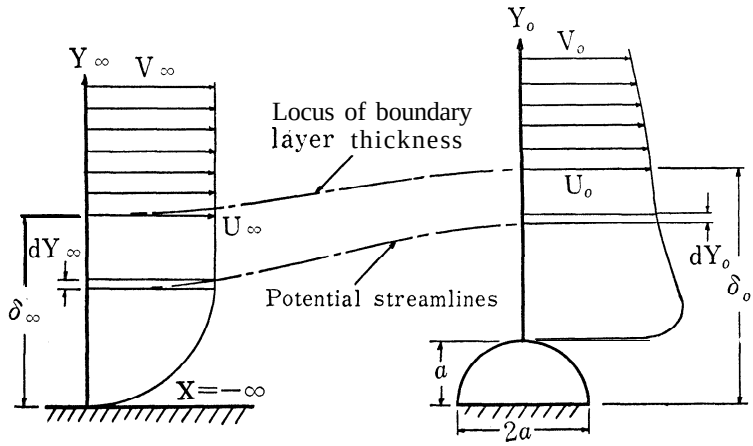

Fig. 12. Flow pictures for the frozen streamline theory.

The frozen streamline theory suggested by Wislicenus[27] assumes that, when a nonuniform flow exists far upstream of **a** semicircular irregularity and the fluid is nonviscous and incompressible, the form of the stream lines is unchanged from that of the uniform potential flow about a cylinder.

As shown in the figure, the stream line through the point $Y_\infty = \delta_\infty$ is the locus of boundary layer thickness, and the flow is irrotational outside and is rotational inside the stream line. At X = 0 and X = $-\infty$ there is no velocity component of Y direction. Therefore, from the continuity condition

$$\frac{U_0}{U_\infty} = \frac{dY_\infty}{dY_0} \tag{38}$$

$$\frac{V_o}{V_\infty} = \frac{dY_\infty}{dY_o} \tag{39}$$

$$\frac{U_\infty}{V_\infty} = \frac{U_o}{V_o} \tag{40}$$

The velocity in the Y direction is 0 at the point X = 0. Thus, denoting the radius of curvature as r for rotational and R for irrotational flow, and denoting the pressure as p for rotational flow and as P for irrotational flow, the below equations are obtained.

$$\frac{d p_0}{d r_0} = \rho \cdot \frac{U_0}{r_0} \tag{41}$$

$$\frac{d P_0}{d R_0} = \rho \cdot \frac{V_0}{R_0} \tag{42}$$

where ρ is the mass density of water. From assumption, r_0 equals to R_0. Therefore,

$$\frac{d p_0}{d P_0} = \left(\frac{U_0}{V_0} \right)^2 \tag{43}$$

from Eq. (40) and (43),

$$dp_0 = \left(\frac{U_\infty}{V_\infty} \right) \cdot d P_0 \tag{44}$$

integrating Eq. (32) from $Y_0 = a$ to $Y_0 = \delta_0$,

$$p_{\delta_0} - p_a = \int_a^{\delta_0} \left(\frac{U_\infty}{V_\infty} \right)^2 d P_0 \tag{45}$$

where p_{δ_0} is the pressure at $Y_0 = \delta_0$ ane p_a is the pressure at $Y_0 = a$. The minimum pressure on a circular cylinder will occur at the point Y_0 = a, so that p_a is the minimum pressure and $p_{\delta_0} = P_{\delta_0}$. It follows

$$P_{\delta_0} - p_{\min} = \int_a^{\delta_0} \left(\frac{U_\infty}{V_\infty} \right)^2 d P_0 \tag{46}$$

Appling Bernoulli's Equation for the potential fields at X = 0

$$\frac{1}{2} \rho \cdot V_0^2 + P_0 = \text{constant} \tag{47}$$

Differentiating Eq. (47) and substituting to Eq. (46),

$$P_{\delta_0} - p_{\min} = -\int_a^{\delta_0} \frac{1}{2} \rho \cdot \left(\frac{U_\infty}{V_\infty} \right)^2 \cdot dV_0^2 \tag{48}$$

Bernoulli's Equation can be applied for the streamline passing $Y_0 = \delta_0$. It yields

$$P_{\delta_0} + \frac{1}{2} \rho \cdot V_{\delta_0}^2 = P_\infty + \frac{1}{2} \rho \cdot V_\infty^2$$

Therefore,

$$P_{\delta_0} = P_\infty + \frac{1}{2} \rho \cdot V_\infty^2 - \frac{1}{2} \rho \cdot V_{\delta_0} \tag{49}$$

Substituting Eq. (49) in Eq. (48),

$$P_\infty - p_{\min} + \frac{1}{2} \rho \cdot V_\infty^2 - \frac{1}{2} \rho \cdot V_{\delta_0}^2 = -\int_a^{\delta_0} \frac{1}{2} \rho \cdot \left(\frac{U_\infty}{V_\infty} \right)^2 \cdot d V_0^2 \tag{50}$$

The minimum pressure coefficient $C_{p\min}$ is given by

$$C_{p\min} = \frac{P_\infty - p_{\min}}{1/2\,\rho \cdot V_\infty^2}$$

Thus, dividing Eq. (50) by $1/2\,\rho \cdot V_\infty^2$ and rearranging it,

$$C_{p\min} = \int_{Q_{\delta_0}}^{Q_a} \left(\frac{U_\infty}{V_\infty}\right)^2 \cdot dQ + Q_{\delta_0} - 1 \tag{51}$$

where

$$Q = \left(\frac{V_0}{V_\infty}\right)^2 \tag{52}$$

Assuming the boundary layer profile is expressed as

$$\frac{U_\infty}{V_\infty} = \left(\frac{Y_\infty}{\delta_\infty}\right)^{1/m} \tag{53}$$

Eq. (51) becomes

$$\begin{aligned} C_{p\min} &= \int_{Q_{\delta_0}}^{Q_a} \left(\frac{Y_\infty}{\delta_\infty}\right)^{2/m} \cdot dQ + Q_{\delta_0} - 1 \\ &= \left(\frac{a}{\delta_\infty}\right)^{2/m} \cdot \int_{Q_{\delta_0}}^{Q_a} \left(\frac{Y_\infty}{a}\right)^{2/m} dQ + Q_{\delta_0} - 1 \end{aligned} \tag{54}$$

From Eq. (32), the stream function of the flow is

$$\psi = V_\infty \cdot Y_\infty \tag{55}$$

at $X = -\infty$,

and

$$\psi = V_\infty \cdot a \cdot \left(\frac{Y_0}{a} - \frac{a}{Y_0}\right) \tag{56}$$

at X = 0.

The stream function is constant along a streamline. Thus, by equating Eq. (55) and (56), it follows that

$$\frac{Y_\infty}{a} = \frac{Y_0}{a} - \frac{a}{Y_0} \tag{57}$$

From Eq. (30), the complex velocity is

$$\frac{dW}{dZ} = V_\infty \cdot \left(1 - \frac{a^2}{Z^2}\right) \tag{58}$$

$Z = i\,Y_0$ at X = 0. Thus,

$$\frac{dW}{dZ} = V_\infty \cdot \left[1 + \left(\frac{a}{Y_0}\right)^2\right] \tag{59}$$

$\frac{dW}{dZ} = V_0$ at X = 0, for the velocity is zero in the Y direction, so that

$$\frac{V_0}{V_\infty} = \left[1 + \left(\frac{a}{Y_0}\right)^2\right] \tag{60}$$

From Eq. (52) and (60)

$$Q = \left[1 + \left(\frac{a}{Y_0}\right)^2\right] \tag{61}$$

$$Q_{\delta_0} = \left[1 + \left(\frac{a}{\delta_0}\right)^2\right]^2 \tag{62}$$

$$Q_a = 4 \tag{63}$$

It is convenient to let $x = \frac{a}{Y_0}$, and $x_0 = \frac{a}{\delta_0}$. Then, from Eq. (57)

$$\frac{Y_\infty}{a} = \frac{1}{x} - x \tag{64}$$

and from Eq. (61), (62)

$$Q = (1 + x^2)^2 \tag{65}$$

$$Q_{\delta_0} = (1 + x_0^2)^2 \tag{66}$$

From Eq. (65), the differential of Q is

$$dQ = 4(x + x^3) \cdot dx \tag{67}$$

Expanding the right hand side of Eq. (66) and subtracting one from both sides of the equation results in

$$Q_{\delta_0} - 1 = 2x_0^2 + x_0 \tag{68}$$

From Eq. (65), $x = 1$ corresponds to Q_a and $x = x_0$ corresponds to Q_{δ_0}. Therefore, from Eq. (54)

$$C_{p\,\min} = 4\left(\frac{a}{\delta_\infty}\right)^{2/m} \cdot \int_{x_0}^{1} \left(\frac{1}{x} - x\right)^{2/m} \cdot (x + x^3) \cdot dx + 2x_0^2 + x_0^4 \tag{69}$$

Rearranging Eq. (69), it follows

$$C_{p\,\min} = 4\left(\frac{a}{\delta_\infty}\right)^{2/m} \cdot \int_{x_0}^{1} x^{3-2/m} \cdot (1 - x^2)^{2/m} \cdot dx + 4\left(\frac{a}{\delta_\infty}\right)^{2/m} \int_{x_0}^{1} x^{1-2/m} \cdot (1 - x^2)^{2/m}\, dx + 2x_0^2 + x_0 \tag{70}$$

This is the general equation for a semicircular irregularity in a turbulent boundary layer having a velocity profile given by Eq. (53). The results of integration of Eq. (70) are[11]
for $m = 1$

$$C_{p\,\min} = 4\left(\frac{a}{\delta_\infty}\right)^2 \cdot \left(\frac{x_0^2}{2} + \frac{x_0^4}{4} - \frac{x_0^6}{6} - \log_e x_0 - \frac{7}{12}\right) + 2x_0^2 + x_0^4 \tag{71}$$

for $m=2$

$$C_{p\,\min} = 4\left(\frac{a}{\delta_\infty}\right)^2 \cdot \left(\frac{4}{5} + \frac{x_0^5}{5} - x_0\right) + 2x_0^2 + x_0^4 \tag{72}$$

for $m = 4$

$$C_{p\,\min} = \frac{3}{8}\left(\frac{a}{\delta_\infty}\right)^{1/2}\left[K - \frac{1}{3}x_0^{7/2}(1-x_0^2)^{1/2} - \frac{7}{15}x_0^{3/2} \cdot (1-x_0^2)^{1/2}\right] + 2x_0^2 + x_0^4 \tag{73}$$

where

$$K = \frac{4}{3}\sqrt{2}\left[2E\left(\frac{1}{\sqrt{2}}, \phi\right) - F\left(\frac{1}{\sqrt{2}}, \phi\right)\right] \tag{74}$$

where E and F are elliptic integrals of the first and second kind respectively, and

$$\phi = \cos^{-1}\sqrt{x_0} \tag{75}$$

Calculated value of $C_{p\,\min}$ for various relative height of roughnesses $\frac{a}{\delta_\infty}$ were shown as Fig. 13 by Holl.[11] Integrations for m = 5, 7 and 10 were carried out by graphical method.

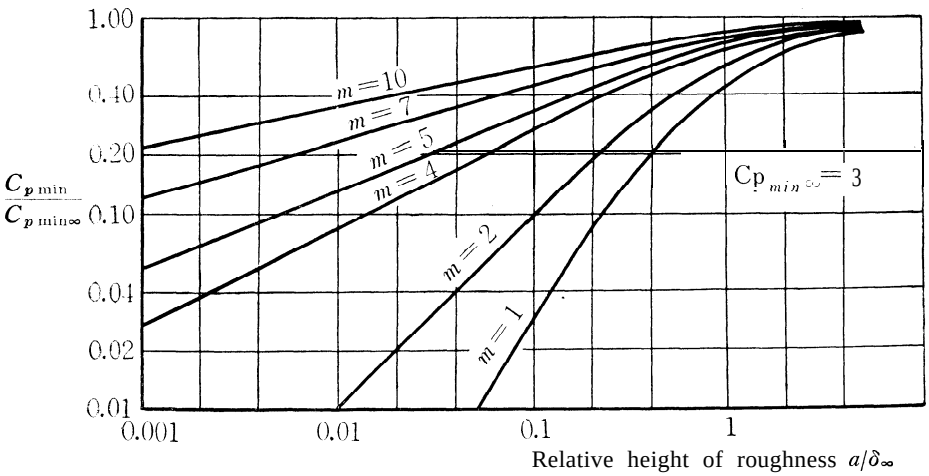

Fig. 13. Normalized minimum pressure coefficient as a function of a/δ_∞.

Previous investigations

A few workers have investigated the onsets of cavitation on isolated surface irregularities. Calehuff and Wislicenus[1] conducted experimental investigation on the onset of cavitation on isolated irregularities using a two dimentional semicircular irregularity. They found that the desinent cavitation number increased with relative

height of roughness $\frac{h}{\delta}$ (h is the height of roughness and δ is the boundary layer thickness) and that it increased with an increase of air content. Walker[27] determined the minimum pressure coefficient of a circular arc shape irregularity theoretically and compared it with the value of σ_a obtained from an experiment. The theoretical prediction of $C_{p\min}$ was 0.840 for the circular arc irregularity, which has a thickness ratio of 0.175 and a relative height of raughness of 0.25, imbeded in a boundary layer which velocity profile was $\frac{U}{V}=\left(\frac{y}{\delta}\right)^{1/8.45}$. His experimental values of $C_{p\min}$ and σ_a were 0.671 and 0.574 respectively. Holl[11] extended the Walker's work and investigated the problem in a wider scope. He carried out an experiment using two families of two dimensional cylindrical roughness elements of constant cross section, i.e. circular arc and triangular. He, also, analized the problem theoretically. He showed that the desinent cavitation number of an isolated surface irregularity imbeded in a turbulent boundary layer was dependent upon the relative height of roughness, the boundary layer shape parameter $H=\frac{\delta^*}{\theta}$ (δ^* the displacement thickness and θ the momentum thickness), the velocity and other unknown variables.

To the author's knowledge, there has not been reported any systematical work concerning the effect of randomly distributed roughness on cavitation beside the report of Kermeen.[15]

III. Design and Construction of 6 inch Water Tunnel

As mentioned previously it is believed no systematical experimental study of cavitation under the influence of randomly distributed surface roughness has been reported. An experimental project on the problem was therefore planned.

Models to be used for the test were to be axially symmetrical bodies having different nose shapes and different surface roughness. The cavitation numbers which will be obtained on different surface roughness will lie in a wide range, so that the free stream velocity and the free stream static pressure in the working section should be controlled in a wide range. A circulating type water tunnel was selected for this reason. The model should be held in the working section by a support. To avoid the effect of the support on the working section flow, the working section length should be relatively long. Therefore, a closed jet type water tunnel would be the suitable type for the test.

Basic design

1. Velocity and static pressure ranges

The important factors which should be discussed in the design of a water tunnel are the ranges of the test section velocity and the test section static pressure.

The test section velocity should cover as wide a range as possible so that the relation between Reynolds number and the cavitation number can be established. For this reason, the higher the maximum test section velocity the better. Considering the test section velocity values of other water tunnels, the maximum test section design velocity was established at 50 ft/sec. The range of the test section velocity should be from zero to the maximum value with the velocity changed gradually within the range. However, the choice of the pump and the motor will determine the velocity variation in the test section.

The test section static pressure can be reduced by setting the test section higher than a datum line where the static pressure is at atmospheric. The maximum elevation above a datum line available in the Hydraulics Laboratory of the Civil Engineering Department, the Pennsylvania State University is 20 feet. This elevation of 20 feet produces a static pressure value of 6 psia in the test section. The available city water line pressure is 85 psia in the Laboratory. The value of 85 psia for the maximum test section static pressure seems to be sufficient for the purpose of the test. From the above considerations, the test section static pressure range was established as the minimum value of 6 psia and the maximum value of the city water line pressure.

2. Test section

The diameter of the test section is determined in connection with the model diameter which is desirable for the test. If the model-to-test section diameter ratio is small, the flow around the model will be influenced by the interference effects from the wall. Yet from the standpoint of cost, the ratio should be small as possible. The ratio used in the high speed water tunnel at the California Institute of Technology is 1 : 5, and in the 48 inch water tunnel at ORL of the Pennsylvania State University 1 :6.[24] The interference effects increase as the diameter of the test section becomes smaller while holding the body size constant. Considering these factors, the ratio of 1 :8 seems to be reasonable for the tunnel. Due to the nature of the investigation, relatively small models can be used. If the test section diameter of 6 inches is used, the suitable diameter of the model is 3/4 inch. The 6 inch size was influenced by the fact that there existed a nozzle

which had a discharge diameter of 6 inches.

Because the other parts of the tunnel have cylindrical cross sections and the models to be used are axially symmetric bodies, the most desirable shape of the test section profile is a circular cross section.

The noses which will be used as models will be attached to a support sting which has a length of 10 1/2 inches. To have some space ahead of the model, the length of the observation part of the test section was set at 24 inches.

It is not desirable for a water tunnel to have a portion in which cavitation will take place during the testing of a model. One of the critical points is the transition section between the test section and the diffuser. To avoid the tendency towards cavitation, the transition section is blended with an approximately 50 1/2 inch radius arc.

3. Pump and motor

The nature of the flow in a closed circuit water tunnel is such that the head loss is relatively small compared to the discharge. The preliminary study of the tunnel losses indicated that at the maximum velocity of **50** ft/sec, a head of 17 to 20 feet would be required. The most effective pump for this condition would be a mixed flow or propeller pump, preferably a mixed flow type. However, the Civil Engineering Department had a 9 inch axial flow propeller pump. Considering the cost saving, it seemed reasonable to use this pump for the tunnel. The pump has four adjustable blades, so that the discharge in the test section could be changed by manually adjusting the angles of the blades.

The edge of the pump blade is the critical location where cavitation is inclined to occur. If profuse cavitation occurs, the efficiency of the pump decreases and the pulsations caused by it disturb the flow. To avoid cavitation there, it is desirable to make the static pressure as high as possible in the pump region. The static pressure at the pump is the sum of three pressures: the test section pressure, the pressure regained in the system resulting from the conversion of kinematic energy to potential energy and the pressure difference caused by the vertical distance between the pump elevation and the test section elevation. The vertical distance should be large enough to avoid cavitation, because the other two conditions are fixed by the test condition. Considering these factors, the location of the pump is just beyond the second turn with a vertical distance of 10 feet between the upper and lower leg center lines.

The test section velocity should have as wide a range as possible as mentioned before. Although the test section velocity can be changed

by adjusting the pump blades, a better way to change velocity is by adjusting the pump speed. While a continuously variable speed drive is desirable, cost again limited the choice to a two speed motor. At the maximum test section velocity of 50 ft/sec, the pump head was estimated as 17.5 feet. Assuming a pump efficiency of 75 percent, the maximum required power of the motor is estimated to be about 25 III?

4. Diffusers and turns

There are two parts in the tunnel where diffusers are employed. One is directly after the test section, while the other is after the pump section. The diffuser has to be designed in such a way that it does not cause poor flow conditions in the tunnel and does not have excessive energy loss. If the diffuser angle is too large, the flow will separate from the wall and cause a high energy loss. On the other hand, if it is too small, the length will become long and the construction expenses will increase. It has been established by an experimental study'") that the suitable diffuser angle can be determined by knowing the area ratio and the entrance condition. Considering these factors, the suitable diffuser angle was established at the range between 5 and 7 degrees.

Two types of turns were considered in the design. One was the so-called miter bend with airfoil type vanes, and the other was a long radius elbow with circular arc turning vanes. Although the first is known to result in an excellent flow condition, the second was decided to be used for the tunnel, after considerations of costs and the purpose of the tunnel.

Dimensions of the tunnel

The tunnel consists of : 1. closed circuit system. 2. tunnel support, 3. pump and drive motor, 4. pressure control system and 5. observation platform. The over all view of the tunnel is shown in Figs. 14 and 15. The closed circuit system which has a height of 10 feet and a width (center to center of the horizontal and verticle legs) of 12 feet and 11 3/8 inches is installed on tunnel supports so that the test section is 15 feet above the floor. An axial flow pump (9 inches in diameter), driven by a two speed motor, is installed to circulate water in the closed circuit system.

1. Closed circuit system

The closed circuit system consists of a working section, a nozzle, diffusers, long elbow turns, and pipes. Joints are connected with welded steel flanges. Sheet packing gaskets, having a thickness of 1/16 inch, are used in all joints. The test section is made from a

plexiglass cylinder which has a 6 inch inside diameter, a 1 inch thickness, and a 2 foot and 3 inch length (observation part is 2 feet). The inside diameter increases from the end of the test section to 10 1/4

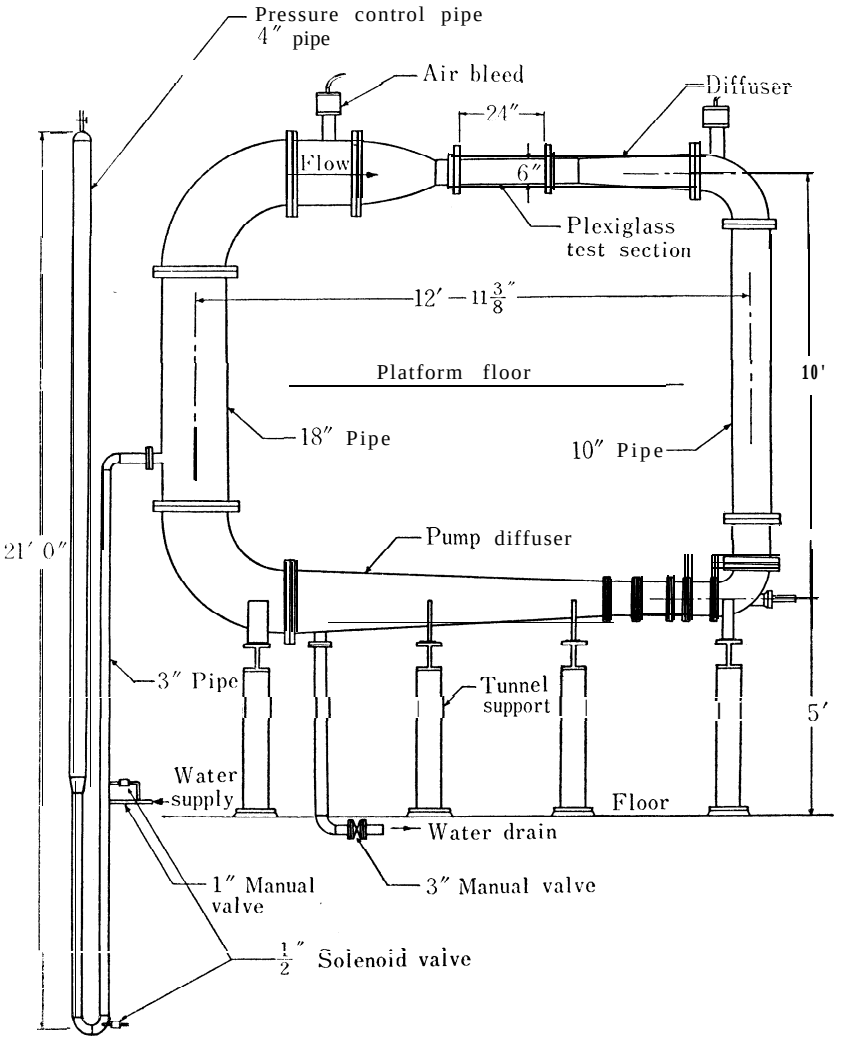

Fig. 14. Six inch water tunnel.

inches through a 2 degree 50 minute steel diffuser having a 3 foot, 4 1/2 inch length and a 1/4 inch wall thickness. The transition part between the test section and a diffuser is blended with a 50 1/2 inch radius circular arc. A sliding joint is installed near the transition

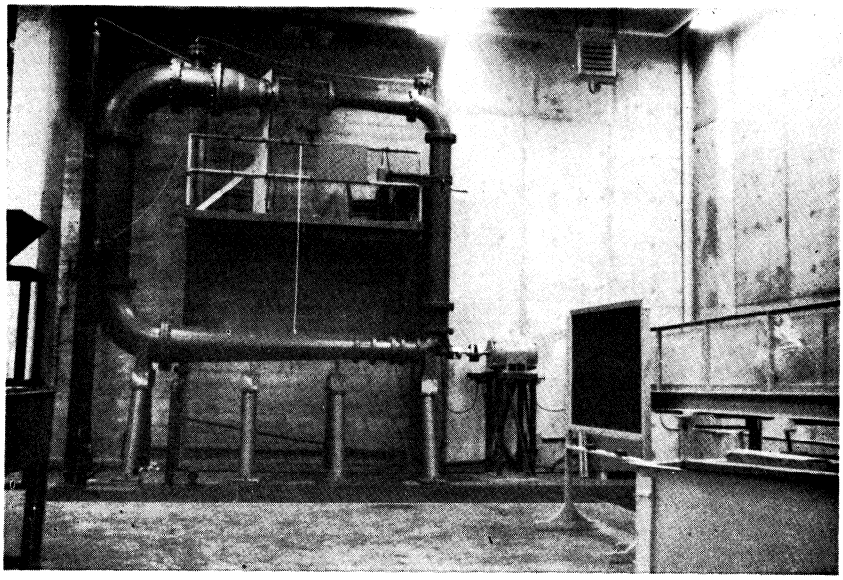

Fig. 15. Six inch water tunnel.

part of the diffuser so that the test section can be removed from the tunnel for model installation **(Fig.** 16.)

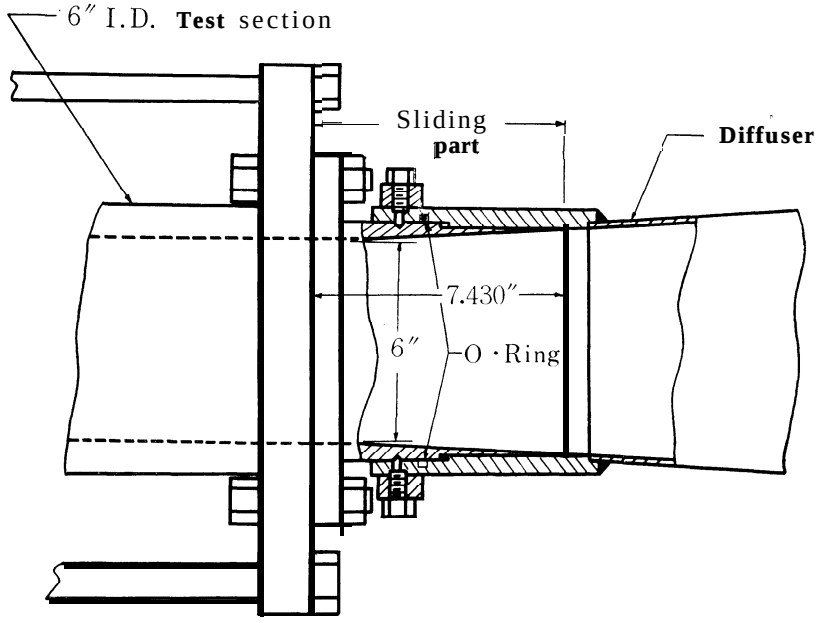

Fig. 16. Sliding joint.

The first turn is a 10 inch diameter standard long radius elbow containing three turning vanes. These were installed to insure good flow conditions as Fig. 17. The vertical leg is a 10 inch diameter pipe (6 feet, 10 1/2 inches in length ; 1/4 inch wall thickness) and is connected to a 9 inch dia. pump elbow by a 10 inch by 9 inch reducing pipe (1 foot 3/10 inch length).

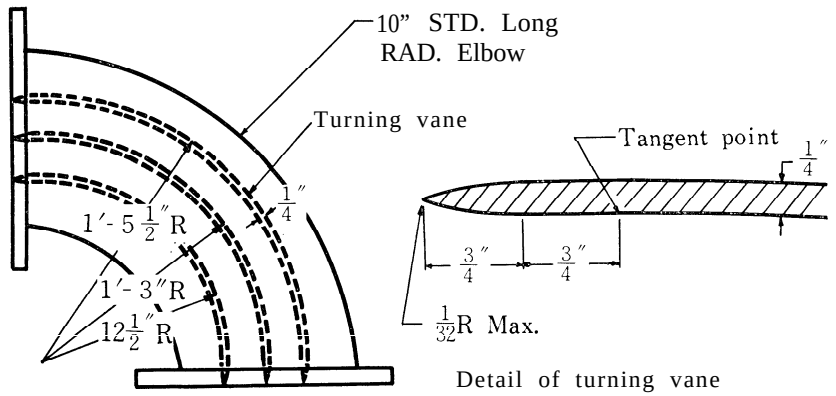

Fig. 17. Turning vane.

The second turn is a pump shaft elbow (9 inches in ID.). To make the pump rotor removable for the adjustment of the blade angle, four pieces of 9 inch ID. steel pipe (entire length is 2 feet, 6 1/8 inches) are provided between the second turn and the pump diffuser as Fig. 18. The pump shaft is contained in the second turn.

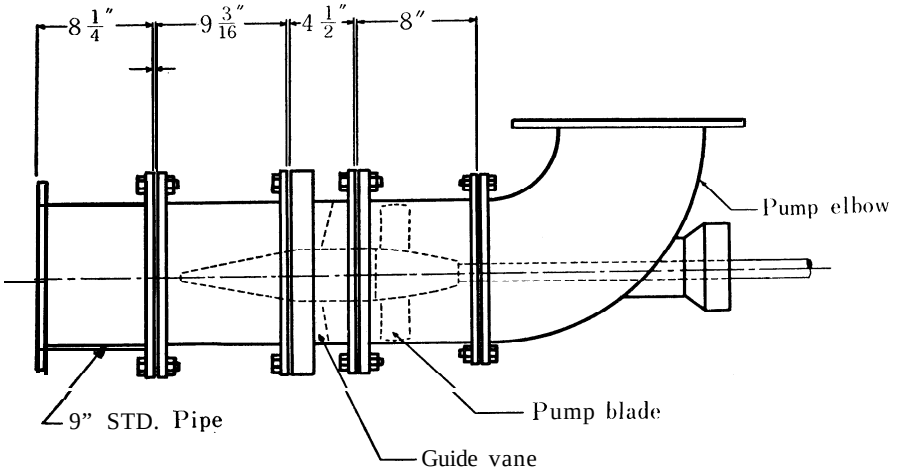

Fig. 18. Pump pipes.

A diffuser having a 7 feet, 4 3/10 inch length, 2 degree, 41 minute angle and 1/2 inch steel wall thickness is connected to the third turn. A tunnel drain pipe (3 inch dia. STD. steel) is welded on the lowest part of the diffuser. The third and fourth turns are 18 inch dia. steel long radius elbows and have three turning vanes.

An 18 inch dia. steel pipe having a length of 4 feet, 5 7/8 inches, connects the third and fourth turns. The pressure control system is connected to it through a 3 inch dia. welded neck flange. There is a horizontal pipe (18 inch dia. steel, 1 foot, 1/16 inch length) and an 18 inch by 6 inch nozzle (cast aluminum, 2 foot, 3 3/16 inch length), between the fourth turn and the test section. Air bleeds are installed on the horizontal 18 inch dia. pipe and the first turn.

The whole structure is supported by four sub-supports which are made from 1/2 inch thick steel plates.

2. Tunnel support

The closed circuit system is placed on four A-frame supports which are made of 6 inch dia. steel pipes, 8 WF 31 structural members and 1 inch base plates. The height of the supports was selected as 3 feet, 10 3/4 inches to make the elevation of the test section center-line 15 feet above the floor. This was as high as practical and was so placed for pressure control reasons as will be discussed later. The typical profile of the supports is shown in Fig. 19.

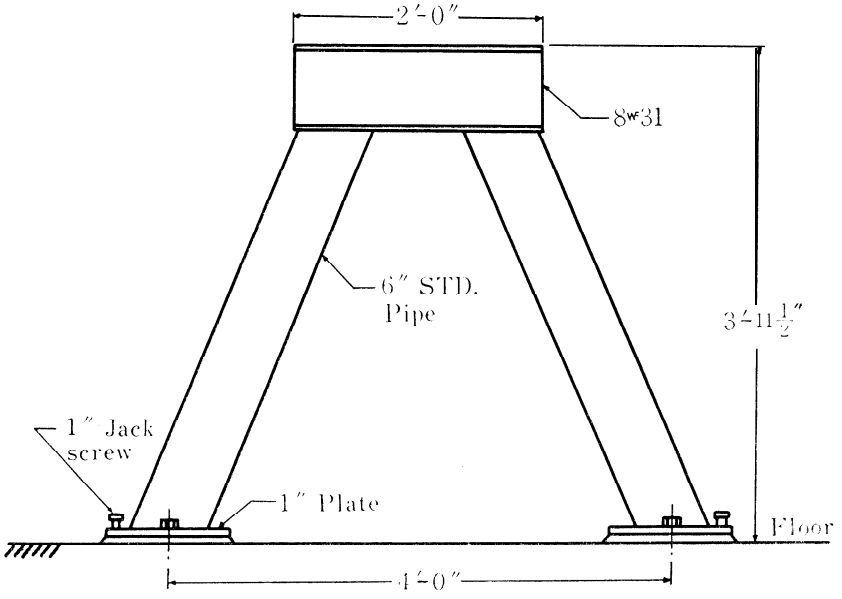

Fig. 19. Tunnel support profile.

3. Pump and drive motor

An axial flow pump (9 inches in diameter, made by S. Morgan Smith Company) is installed on the second turn as mentioned before. The pump rotor has four blades with manually adjustable angles to obtain different discharges. A flexible coupling connects the pump shaft directly to the motor. The drive motor used is a Westinghouse AUDP two speed motor (25 HP-1180 RPM, 14 HP-885 RPM).

4. Pressure control system (Fig. 20)

This system consists of a vertical pipe and the connecting pipe line. The vertical pipe is made of a 4 inch dia. pipe (15 feet, 7 inches in length, upper part) and a 3 inch dia. pipe (5 feet, 5 inches in length, lower part) which are connected together with a 4 inch by 3 inch reducer. The top is closed with a 4 inch cap. A 1/4 inch needle valve is installed on the plastic pipe line which is connected to the top of the cap. The elevations cf the top and the bottom of the main vertical pipe are 16 feet above the floor and 5 feet below the floor, so that the entire height is 21 feet.

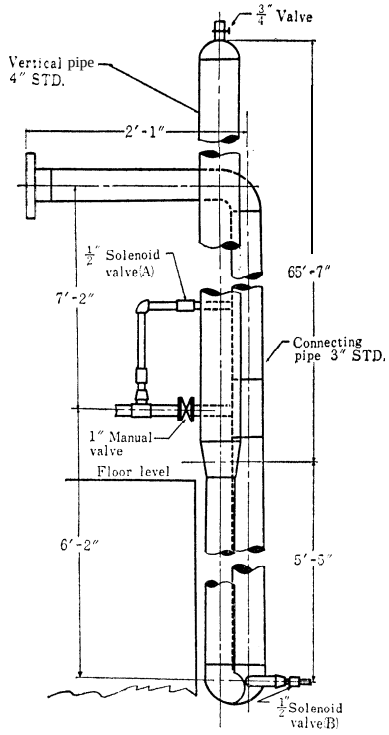

Fig. 20. Pressure control system.

A 3 inch dia. steel pipe connects the lower extremity of the pressure control system to the main tunnel. At the bottom of the main vertical pipe a 1/2 inch solenoid valve is installed to control the water drain. City water is supplied through the 1 inch dia. pipe which is welded to the connecting pipe line. The water supply is controlled by a 1 inch dia. gate valve and 1/2 inch dia. solenoid valve.

5. Observation platform

The platform is a welded steel structure which is made of 8 inch by 2 1/4 inch channels, 6 inch by 2 1/2 inch channels, and 4 by 4 angles. The top is covered with Type L21 Blaw-Knox Electroforged Grating. **The** area and the elevation of the top surface are 9 feet, 6 inches by 6 feet, 4 inches plus 2 feet by 5 feet, 6 inches and 10 feet above the floor.

Expected hydraulic conditions

1. Tunnel losses

The loss in the tunnel may be broken down as (a). working section loss, (b). diffuser losses, (c). turn losses and (d). losses due to straight pipes. Since the tunnel is made of sections of various diameters, it may be convenient to express these losses on the basis of the test section velocity head as follows

$$h = K\left(\frac{A_0}{A}\right)^2 \frac{V_0^2}{2g} = K' \frac{V_0^2}{2g} \tag{76}$$

where

h: head loss at a section in question
K: loss coefficient at a section in question
A: area of the section
A_0: velocity at the test section
V_0: velocity at the test section
g: acceleration of gravity
K': loss coefficient expressed on the basis of the test section velocity head

(a). Working section loss

The theoretical and experimental study of 48 inch water tunnel working section flow[18] has concluded that the working section loss can be computed as being equivalent to the loss in the entrance region of a straight pipe having an effective length equal to that of the working section, plus half of the transition section and plus the effective length of the nozzle which is about one diameter.

The effective length of the tunnel working section will be 5.5 diameters, if it is assumed to be the sum of the effective length of the nozzle (one diameter) and entire test section length (2 feet, 3 inches). Based on the theoretical calculation by ORL water tunnel[18] and using the above value, the pressure head loss of the test section is computed to be 0.098 test section velocity heads for a test section Reynolds number of 2×10^5 (near maximum velocity).

(b). Diffuser losses

Although no theory which satisfactorily handles diffuser flow losses has been found, some interesting experimental work has been done at ORL.[19] It concluded that the diffuser pressure efficiency was a function of the total diffuser angle, the working section Reynolds number. Also, the working section Reynolds number had little effect on the pressure efficiency at Reynolds number above 10^5 and at diffuser angles of 7.5 degrees or less. The Reynolds number and diffuser angle for

the first diffuser are 2 × 10" and 5 degrees, 40 minutes, respectively. The diffuser loss is predicted at 0.124 test section heads. The loss due to the second diffuser is included in the above value.

(c). Turn losses

Considering three long sweep elbows, the total turn loss was calculated at 0.349 test section velocity heads. Since the turns have turning vanes, the flow condition should be improved and the loss should decrease. Taking this into consideration, the head loss is predicted as 0.250 test section velocity heads.

(d). Losses due to straight pipes

The losses in all the remaining straight pipes can be calculated in the usual manner. The predicted value is 0.048 test section velocity heads.

The total loss of the tunnel is thus 0.520 test section velocity heads.

2. Maximum test section velocity

The maximum test section velocity can be obtained from the maximum motor output power, the pump efficiency and the tunnel loss coefficient. Using a 25 HP motor, and taking the pump efficiency as 75 percent and the loss coefficient as 0.520 test section velocity heads, the maximum tunnel velocity is calculated at approximately 47 feet/sec.

3. Test section static pressure

As mentioned before, the test section static pressure is controlled by the pressure control system. An increase in the test section static pressure is obtained by opening the water supply solenoid valve (A) (of Fig. 20) while closing other valves. Therefore, the maximum value of the test section static pressure is the city water line pressure of about 85 psia.

The test section static pressure is decreased by opening the solenoid valve (B) (of Fig. 20). The minimum value obtained is the difference of the atmospheric pressure and the pressure value which corresponds to the maximum effective height of the pressure control system. The maximum effective height is the vertical distance from the test section centerline to the lowest elevation of the free surface in the pressure control system. The test section centerline is 15 feet above the floor and the free surface is 5 feet below the floor, so that the maximum effective height is 20 feet, corresponding to the static pressure value of 6 psia in the test section.

Proofing of circuit

1. Test section velocity

As mentioned before, the test section velocity can be changed by adjusting the motor speed (or the pump blade angle). The velocity was determined by reading the differential manometer head across the nozzle. To assure that the flow condition in the test section was the same as that at which the test was to be undertaken, a 1.5 caliber ogive smooth nose was installed in the test section. After trying a number of pump blade angles, it was determined that an angle of 36 degrees produced the maximum velocity. At this setting the high and low motor speeds corresponded to 43.52 feet per second and 32.42 feet per second respectively. Because it was difficult to obtain cavitation on the ogive noses at the lower velocity, and higher velocities could not be obtained, this blade angle was used for the test.

2. Pressure control system

Static pressure values in the test section were measured by reading a precision Burdon tube pressure gage which was connected to the beginning of the test section.

Test section static pressure was increased by opening valve (A) (of Fig. 20) until it reached the maximum value. The increase of static pressure was very fast and the impact forces of opening and closing of the valve caused rapid variations of static pressure. Therefore, a 1/4 inch manual needle valve was installed. Operating this valve permitted small pressure increases.

The decrease of test section static pressure was controlled by operating the switch for the valve (B). Although the designed minimum static pressure of 6 psia was reached by doing so, this value was not quite low enough for the occurrence of cavitation on the smooth ogive nose at the low test section velocity. Therefore, a vacuum pump was connected to the top of the pressure control pipe to reduce the static pressure. The minimum static pressure in the test section dropped to about 2 psia with this value sufficient for the test purpose.

Operation of the tunnel

To install a model in the test section, the test section is first removed from the tunnel. A small overhead crane is used to support the test section during this operation. First, the 1/2 inch screws which were installed on the sliding joint to resist the sliding are loosened. Then, the tie rod which ties the test section and the diffuser together to prevent opening of the sliding joint is removed. The test section can now be taken out by first pulling out the dowel pins and removing the bolts which tie the end flanges of the test section and

adjoining flanges together. The test section can then be removed from the tunnel by slowly operating the crane. Once the test section is removed, a model can be installed in the test section by reaching in through the ends.

The process of putting the test section back is the reverse of the removal process. First, position the test section to the proper position, install the dowel pins and replace the bolts. Then fasten the tie rod joining the diffuser section and the test section. Finally tighten the screws on the sliding joint.

To remove the pump blades, the 9 inch dia. pipe next to the pump diffuser should be removed first. Then, the other pieces of 9 inch pipes are removed. By doing so, the pump can be taken off and the blade angle can be adjusted.

The main valve for city water supply is located at the north east corner of the Hydraulic Laboratory. The tunnel can be filled with water by opening the water supply valve on the tunnel and also opening both air bleeds to permit air to escape from the tunnel circuit. The pressure control vertical pipe is closed at the top while filling the tunnel with water. When the water level reaches about the center line of the upper leg, the large valve is shut off and the remainder of the water added through the use of the 1/2 inch solenoid supply valve. The switch for the solenoid valve was installed on the platform. After the tunnel was filled with water, the valves of the air bleeds were closed and the water was circulated several times prior to releasing free air through the air bleeds.

The main motor switch is located on the wall close to the motor. After turning the main switch on, starting and stopping the motor can be controlled by using the motor switch which was installed on the platform.

The pressure gage should be adjusted to the atmospheric pressure value for each day. The adjustment is done by moving the adjusting screw on the pressure gage. Also, care should be taken to insure that all air bubbles in the small tube connecting the pressure gage to the test section are removed.

IV. TEST

The purpose of the test is to investigate the problem of "'the effects of distributed surface roughness on cavitation." Axially symmetrical models having different surface roughness were selected for the purpose. Desinent and incipient cavitation numbers expressed as Eq. (7) and (8) were found for each model, using the 6 inch water tunnel. Furthermore, the effect of air content on cavitation was in-

vestigated experimentally.

Models

The models employed in the test were three families of 3/4 inch diameter stainless steel noses having 1.5 caliber ogive, hemispherical and blunt profiles (Figs. 21, 22). Each family consists of four noses having different surface roughness. In testing, the nose is installed in the test section by being screwed into the end of a sting. The sting has a length of 10 2/2 inches and is supported in the test section by a plexiglass sting support so that the axis of the nose coincides with the centerline of the tunnel test section. The detail of the supporting structure is shown in Fig. 23.

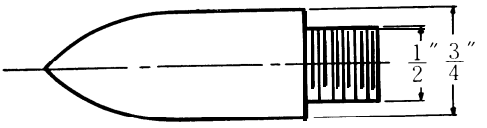

1.5 Caliber ogive

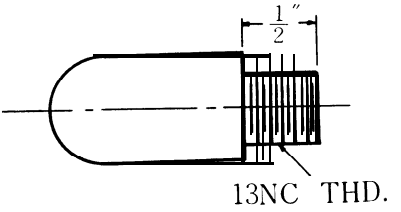

Hemispherical nose

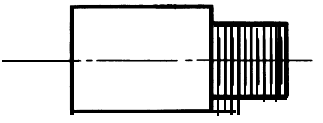

Blunt nose

Fig. 21. Nose shape.

An experimental study on cavitation scale effects of smooth 1.5 caliber ogive noses and hemispherical noses has been reported by B. R. Parkin and J. W. Holl.[20] In selecting the 1.5 caliber ogive and hemispherical noses, the data on smooth noses can be compared with this data. A blunt nose was also selected (0 caliber ogive), because the effect of surface roughness should be larger than on other noses as the boundary layer would be extremely thin at the edge of the nose.

Surface roughness was produced on models in such a way that roughness was scattered as randomly and yet as uniformly as possible. The first roughness was finished smooth by polishing, the second roughness was produced by sand blasting, while the other two were produced by blasting with steel shot. Surface roughness was measured along the lines parallel to the centerlines of models using a Brush Model BL-103 Surface Analyzer. The Analyzer measures the height of roughness directly in inches and, at the same time μ inch rms value. Data obtained are shown in Figs. 24-27. Average surface

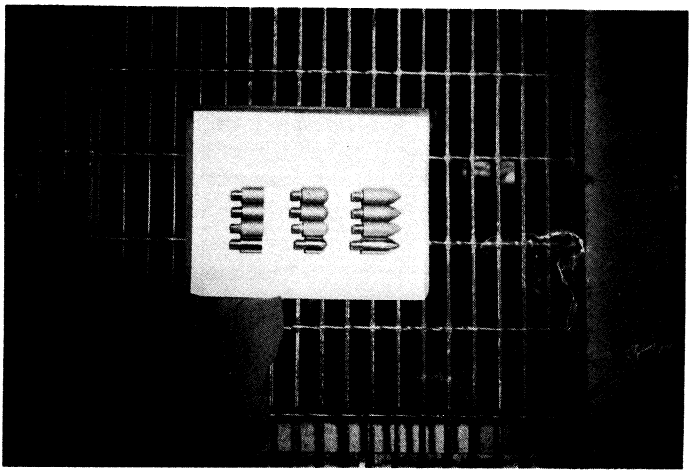

Fig. 22. Models.

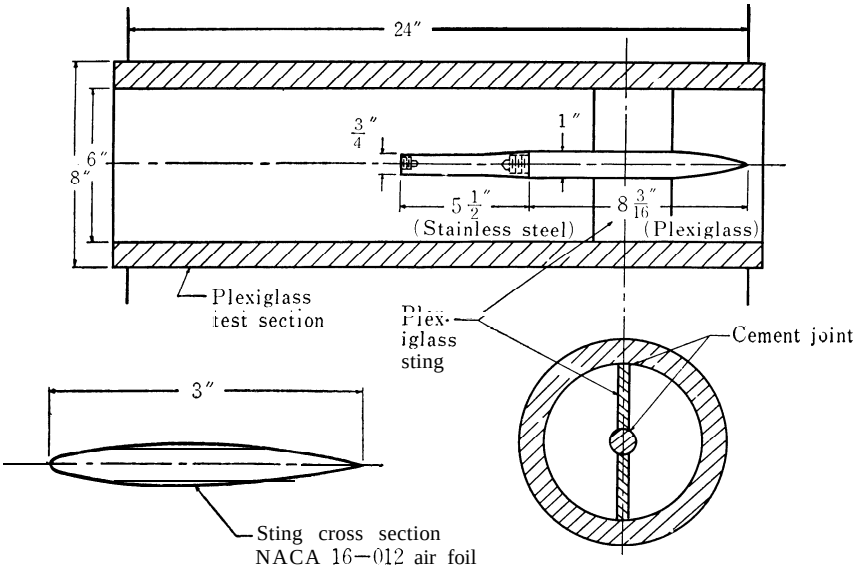

Fig. 23. Model support.

roughness in μ inch rms for each nose are as follows. For 1.5 caliber ogive noses, the first roughness is 10, the second is 120, the third and fourth are 305 and 335 μ inches rms respectively. For hemispherical noses, they are 2.8, 75, 560 and 550 μ inches rms. For blunt noses, they are **5, 84, 440** and **580** μ inches respectively.

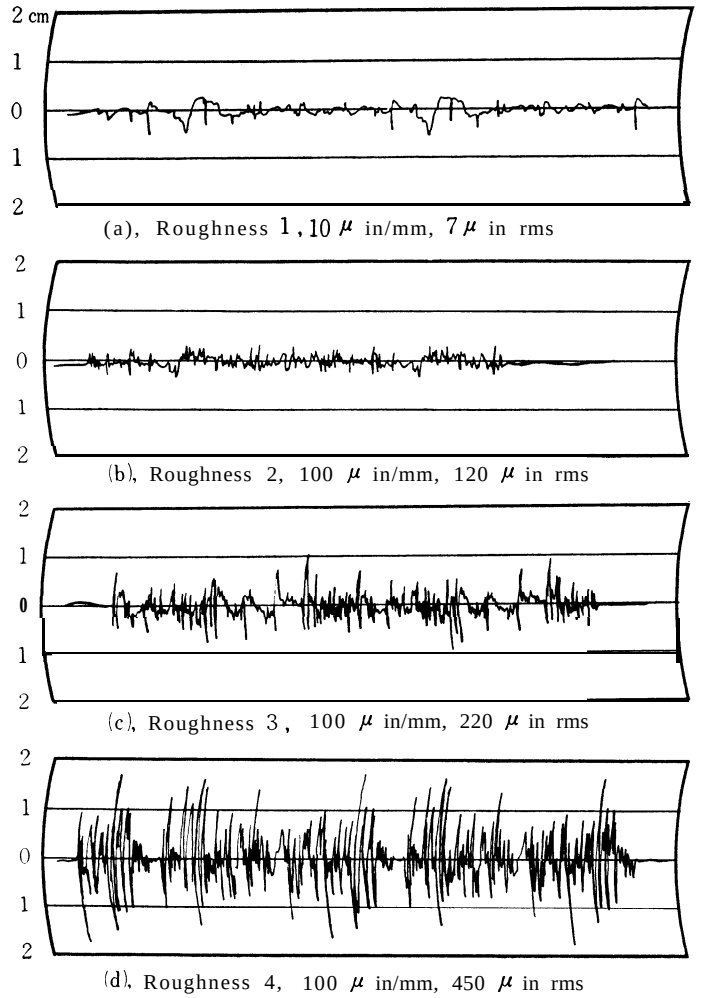

Fig. 24. Surface roughness for 1.5 caliver ogive noses.

The test technique was as follows. A model was placed in the test section, the tunnel was filled with fresh water, and the pressure page set at the atmospheric pressure obtained from a barometer reading.

Keeping the test section velocity constant, the inception cavitation pressure P_i and the desinent cavitation pressure P_d were measured by reading the pressure gage. The incipient cavitation was obtained by

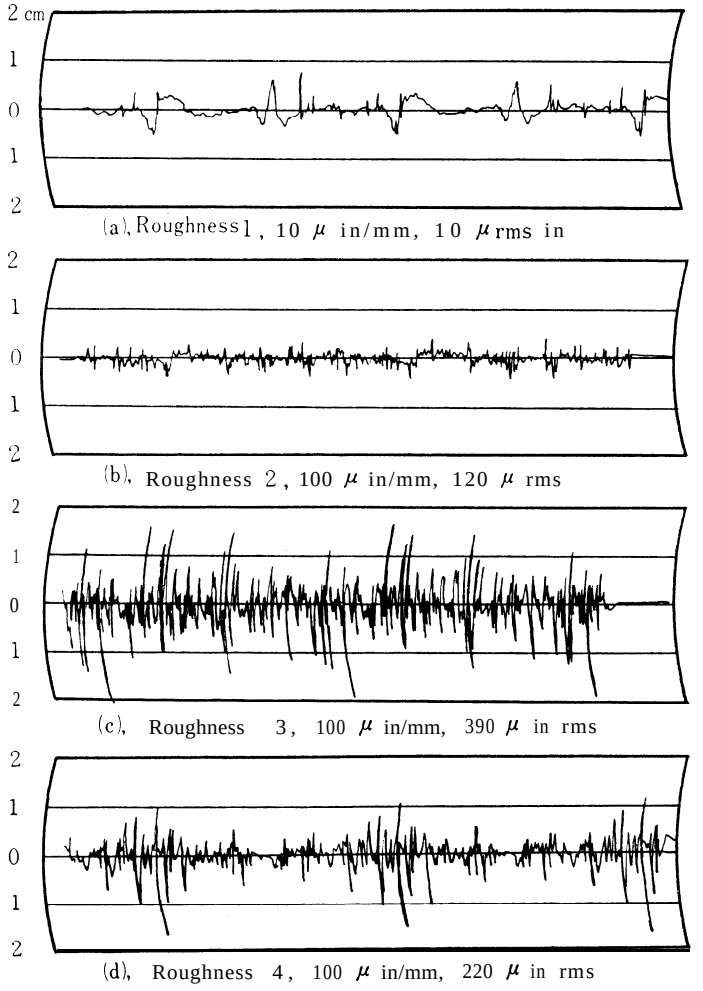

Fig. 25. Surface roughness for 1.5 caliver ogive noses.

lowering the static pressure from the non-cavitating flow regime and observing the first appearance of cavitation, while the desinent cavitation was reached by first establishing a cavity flow and raising the static pressure slowly to determine the disappearance of the last bit of cavitation. Five pressure observations were made under the same

condition to be sure the value was a true representation of cavitation and to check the repeatability of cavitation. Changing the test section velocity, the same observations were then made.

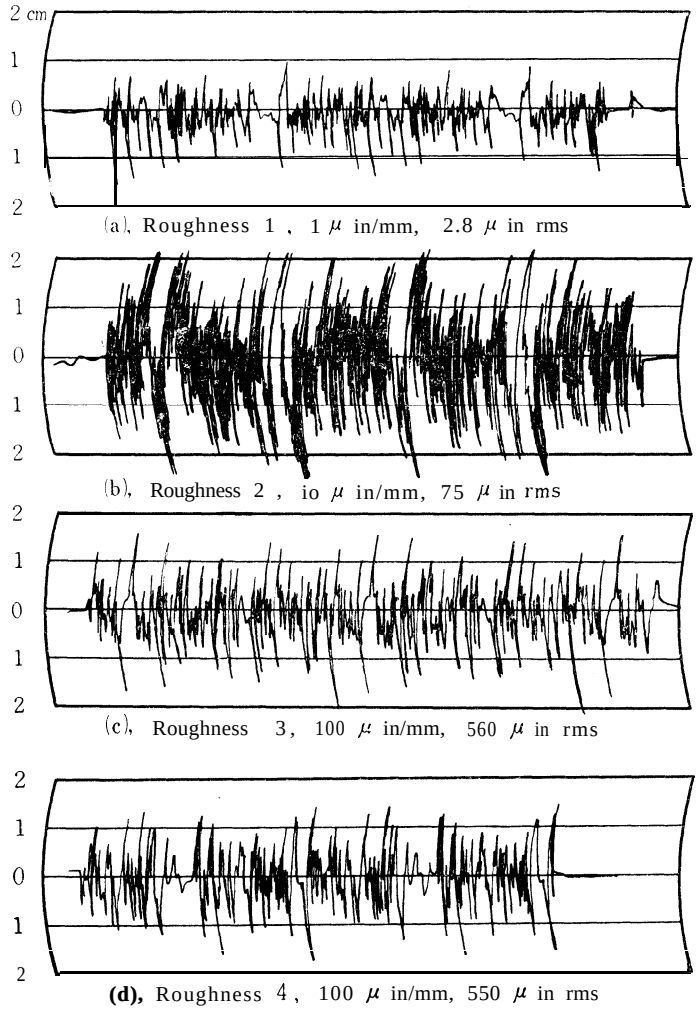

Fig. 26. Surface roughness for hemispherical noses.

After this operation was over, a water sample was extracted from the tunnel through a plastic tube connected to the air bleed. Using **a** pyrex glass bottle, the sample was removed making sure that free air did not mix into the sample. The air content was obtained by using the Van Slyke equipment at the Ordnance Research Laboratory. The

air content was expressed in ppm values (parts per million by molecular weight of air to water). The water temperature was also measured for each test run.

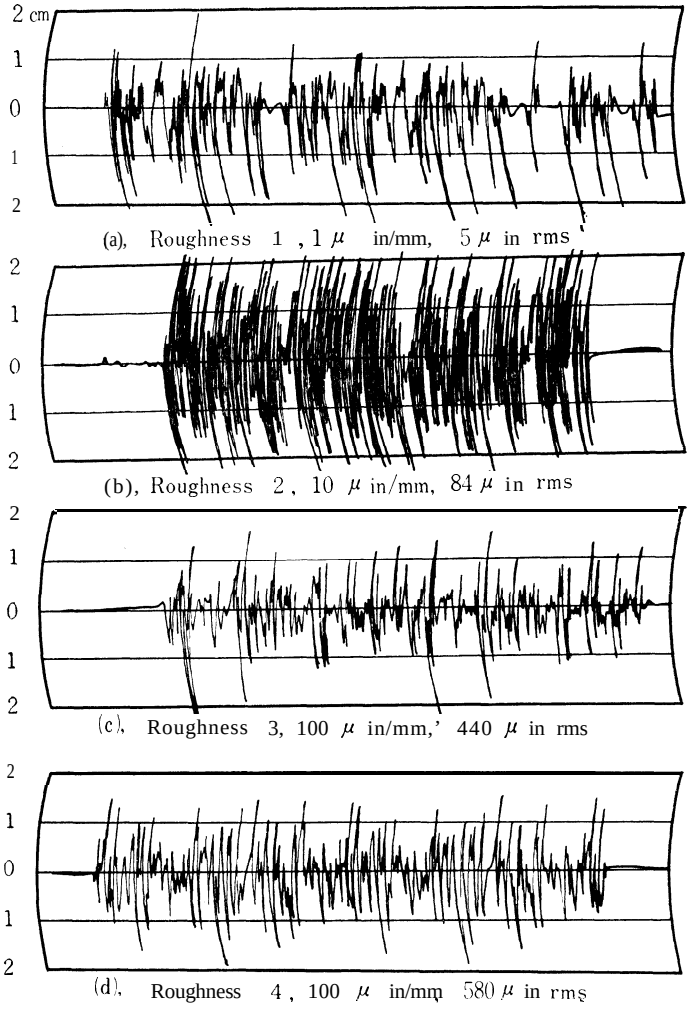

Fig. 27. Surface roughness for blunt noses.

As the next step, the air content of water was lowered to a certain value by using a small vacuum pump connected to both air bleeds. To permit more rapid air removal, the water surface was dropped to about half the height of the test section diameter. The water was circulated occasionally so that "new" water became exposed to the

free surface under vacuum. Then, the same operation of test as described above was conducted. Each series of tests consisted of five to seven test run covering five to seven variations of air content. The air content ranged from about 2 to 22 ppm per mole weight. In addition, a test consisting of twelve observations of desinent cavitation pressure were made for a nose, keeping the air content around 5 to 6 ppm per mole weight. By this test, the desinent cavitation value was assured and the comparison of the values among different surface roughness became possible.

A series of tests was completed by conducting the same procedure on four different surface roughness. Series I is for 1.5 caliber ogive, series II for hemispherical and series III for blunt noses.

V. Test results

Data obtained

Knowing the test section velocities and recording the test section static pressures for desinent and incipient cavitation, the desinent cavitation number σ_d and the incipient cavitation number σ_i for each nose and for each air content were calculated. The relation between the desinent cavitation number and air content, and the incipient cavitation number and air content were plotted for each series of tests.

Figs. 28-31 show these relationships for 1.5 caliber ogives noses while Figs. 34-37 are for hemispherical noses and Figs. 40—43 for

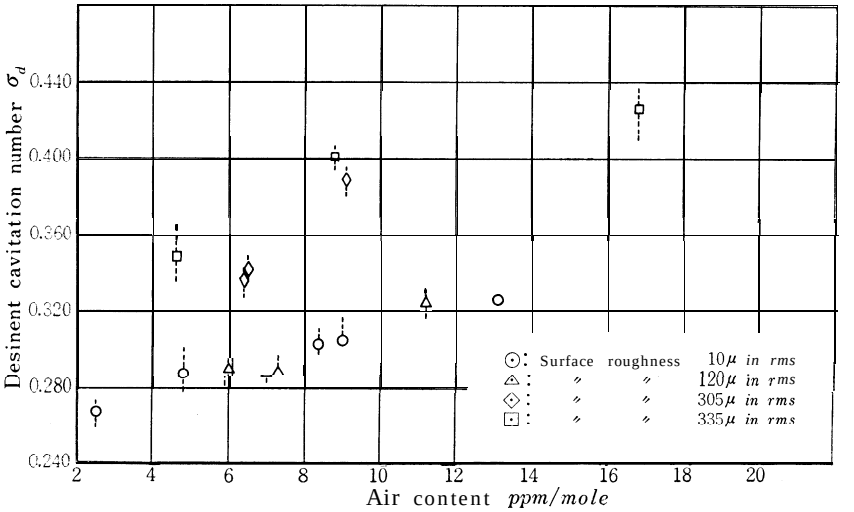

Fig. 28. Desinent cavitation number vs air content for caliber 1.5 ogive nose (V_0 = 32.42 ft/sec).

blunt noses, respectively. On the figures, the circle, triangle, diamond and square symbols represent the average values of cavitation numbers of five observations for different surface roughness. The circle symbol is for the smooth finish, the triangle is for second roughness, while the diamond and square are for the third and fourth surface roughness

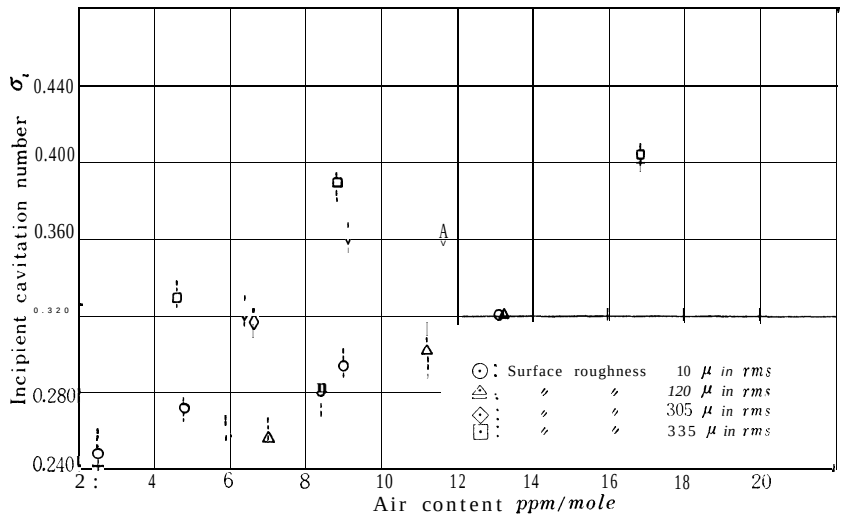

Fig. 29. Incipient cavitation number vs air content for caliber 1.5 ogive nose (V_0 = 32.42 ft/sec).

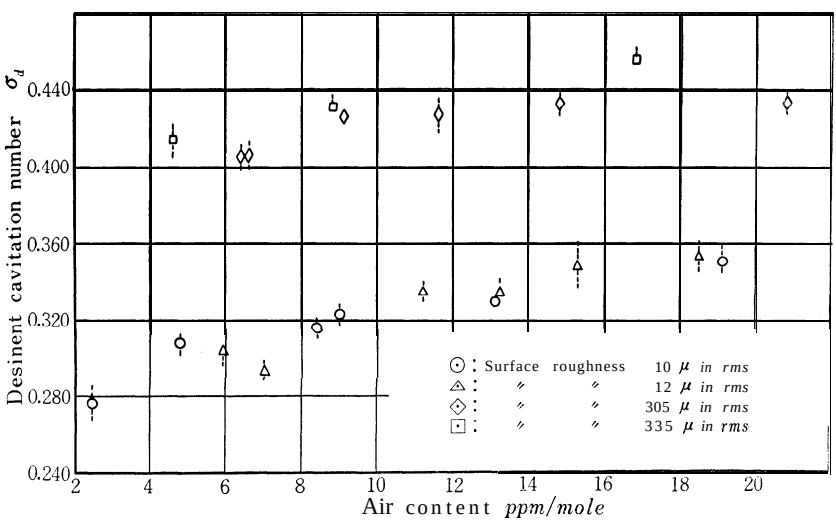

Fig. 30. Desinent cavitation number vs air content for caliber 1.5 ogive nose (V_0 = 43.52 ft/sec).

respectively. Vertical dotted lines through each symbol represent the scatter of the five separate observations.

To compare the desinent cavitation number for different surface roughness, twelve observations of desinent cavitation were plotted

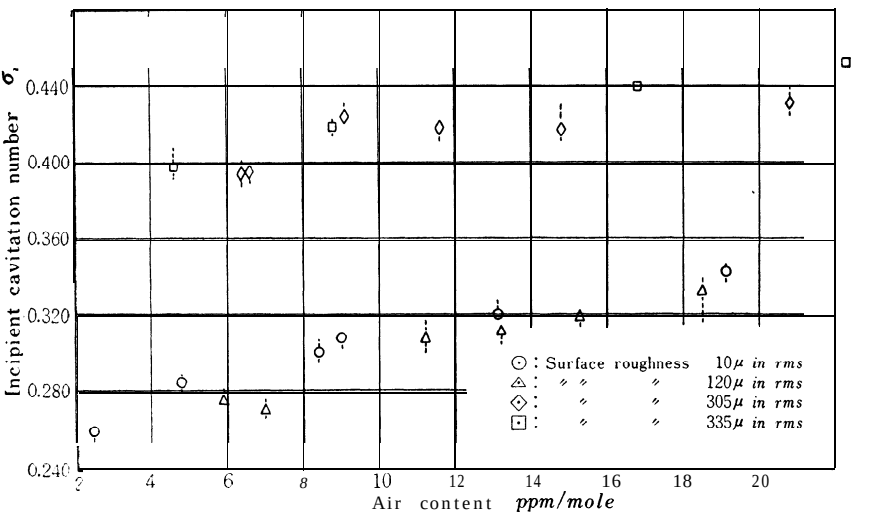

Fig. 31. Incipient cavitation number vs air content for caliber 1.5 ogive nose (V_0=43.52 ft/sec).

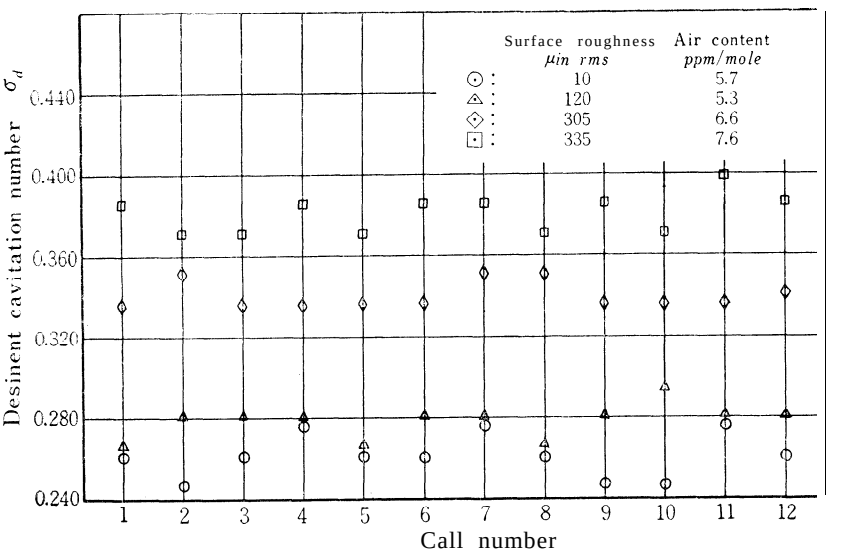

Fig. 32. Desinent cavitation number for caliber 1.5 ogive nose (V_0 = 32.42 ft/sec).

against the observation number, for each test section velocity and for each nose shape. Figs. 32 and 33 are for 1.5 caliber ogives, Figs. 38 and 39

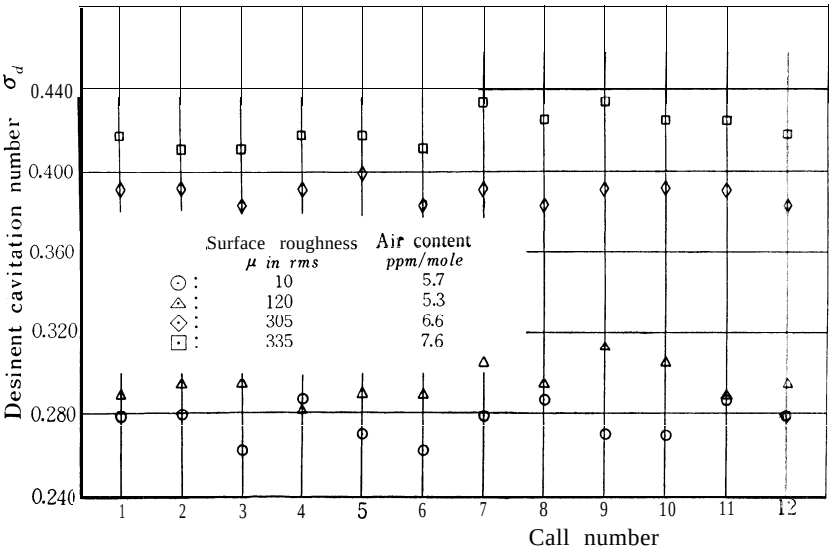

Fig. 33. Desinent cavitation number for caliber 1.5 ogive nose (V_0 = 43.52 ft/sec).

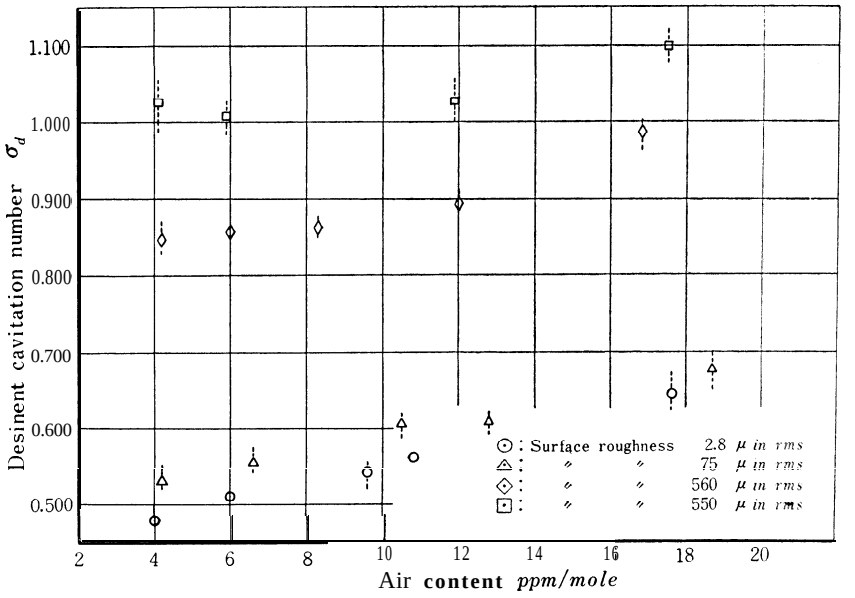

Fig. 34. Desinent cavitation number vs air content for hemispherical nose (V_0 = 32.42 ft/sec).

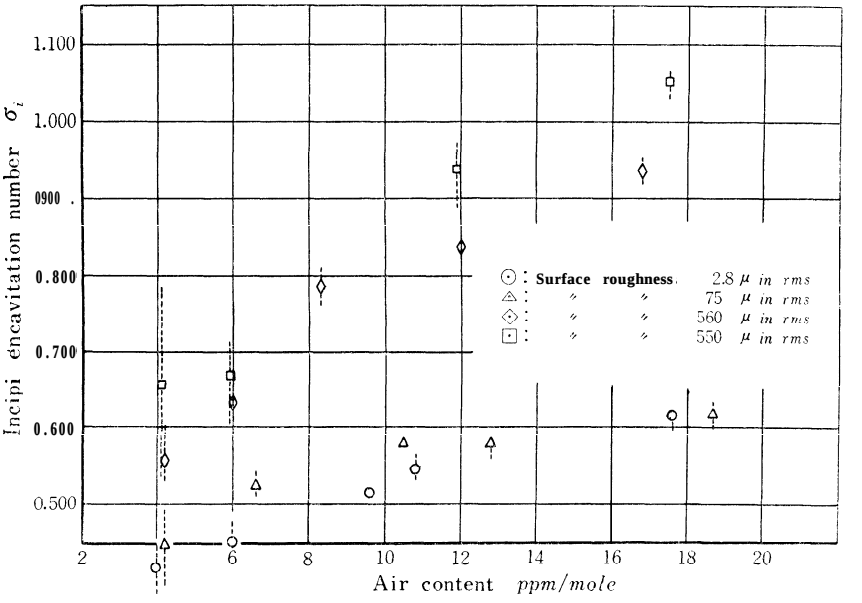

Fig. 35. Incipient cavitation number vs air content for hemispherical nose (V_0=32.42 ft/sec).

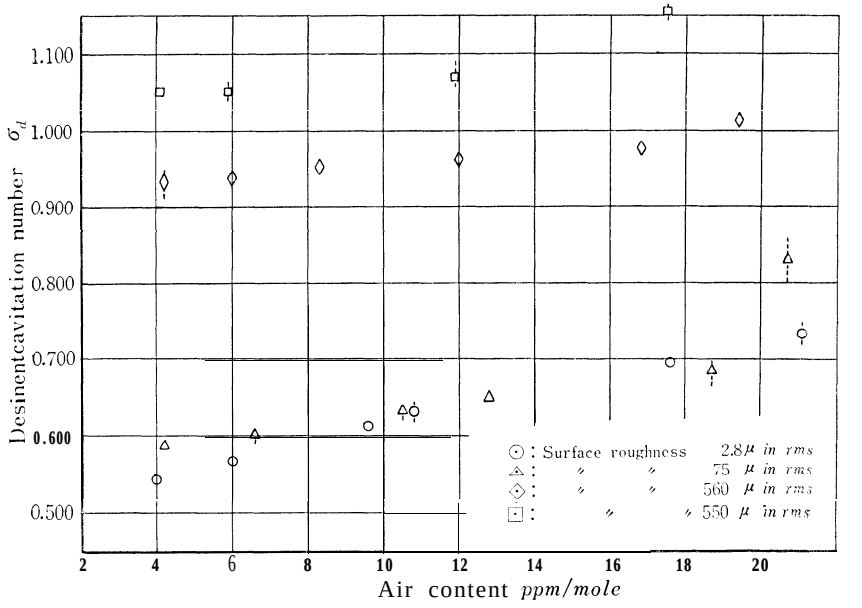

Fig. 36. Desinent cavitation number vs air content for hemispherical nose (V_0=43.52 ft/sec).

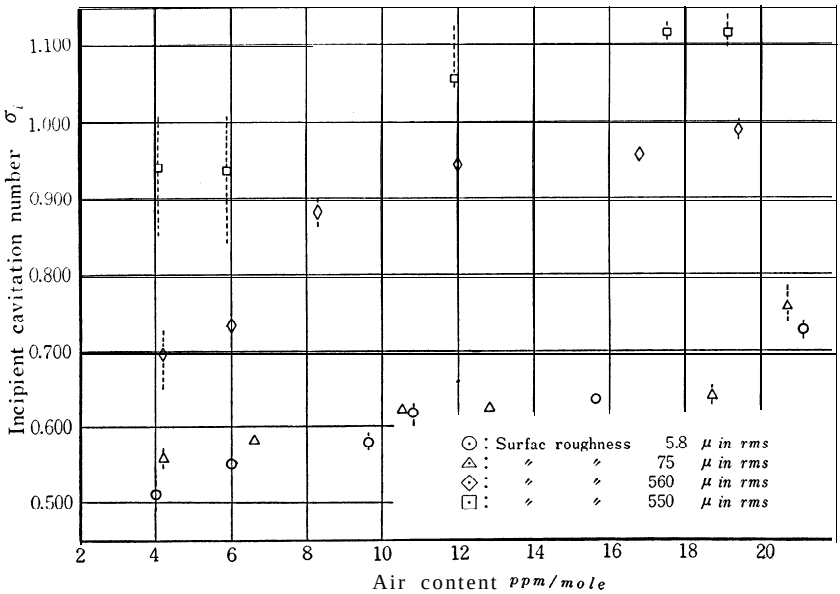

Fig. 37. Incipient cavitation number vs air content for hemispherical nose (V_0=45.52 ft/sec).

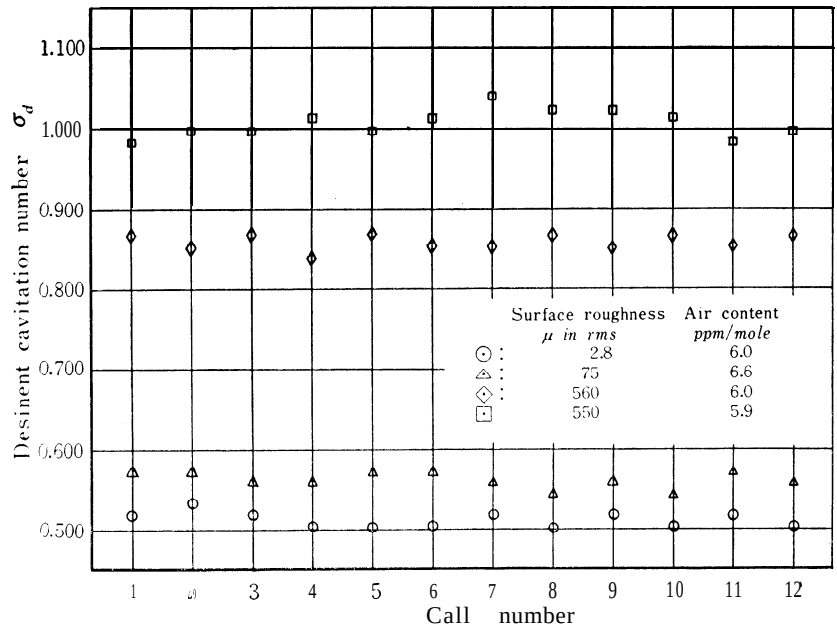

Fig. 38. Desinent cavitation number for hemispherical nose (V_0 = 32.42 f t/sec).

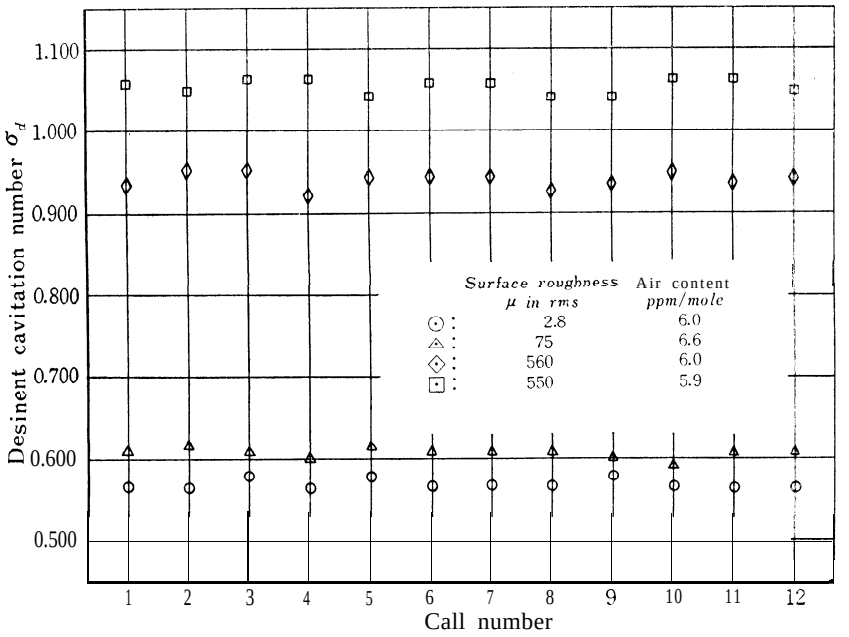

Fig. 39. Desinent cavitation number for hemispherical nose (V_0=43.52 ft/sec).

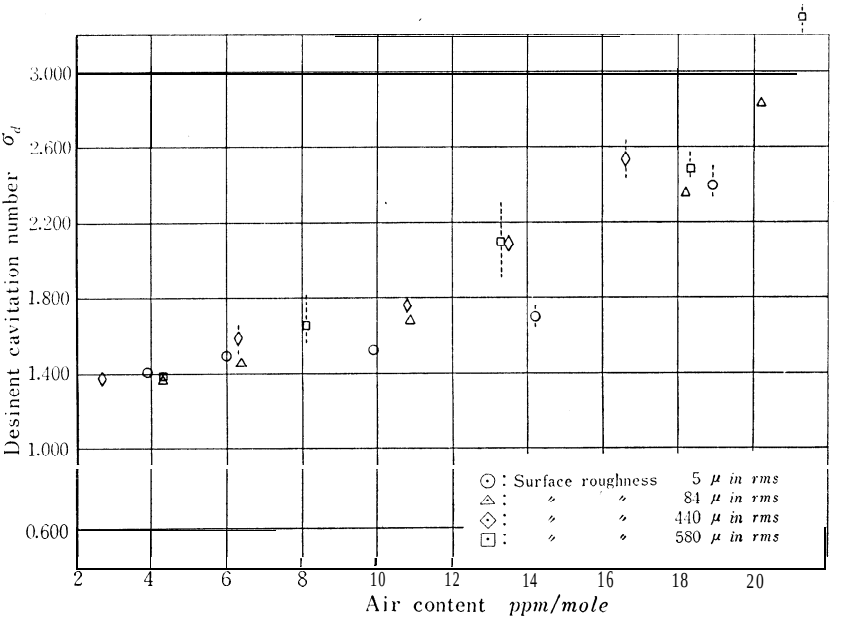

Fig. 40. Desinent cavitation number vs air content for blunt nose (V_0= 32.42 ft/sec).

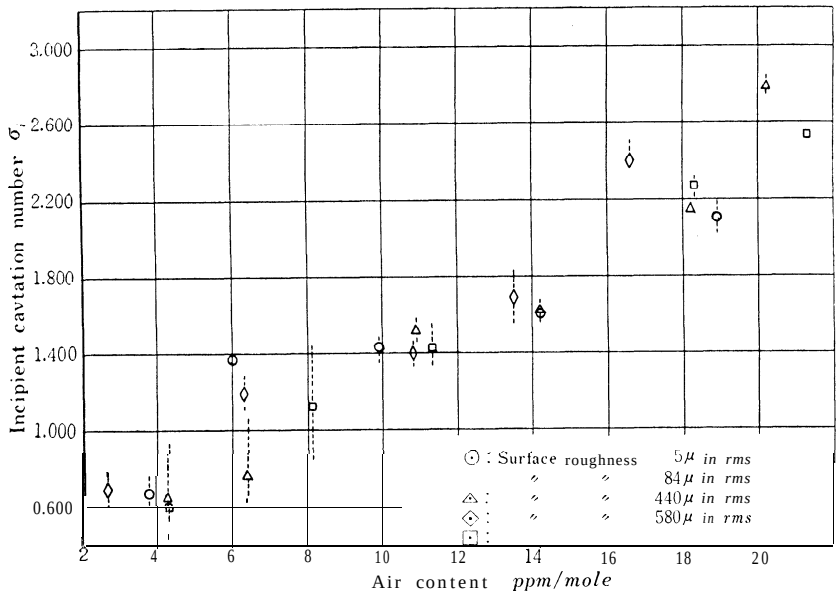

Fig. 41. Incipient cavitation number vs air content for blunt nose (V_0=32.42 ft/sec).

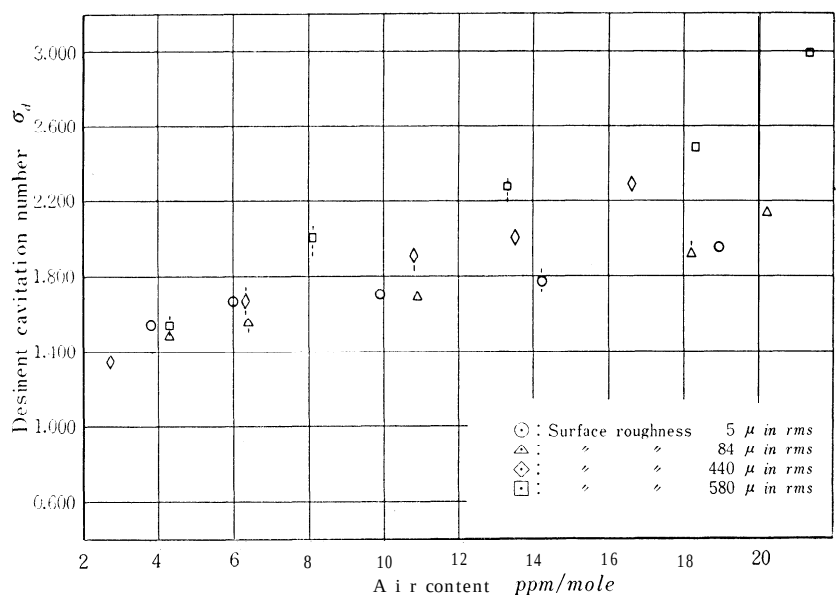

Fig. 42. Desinent cavitation number vs air content for blunt nose (V_0 = 43.52 ft/sec).

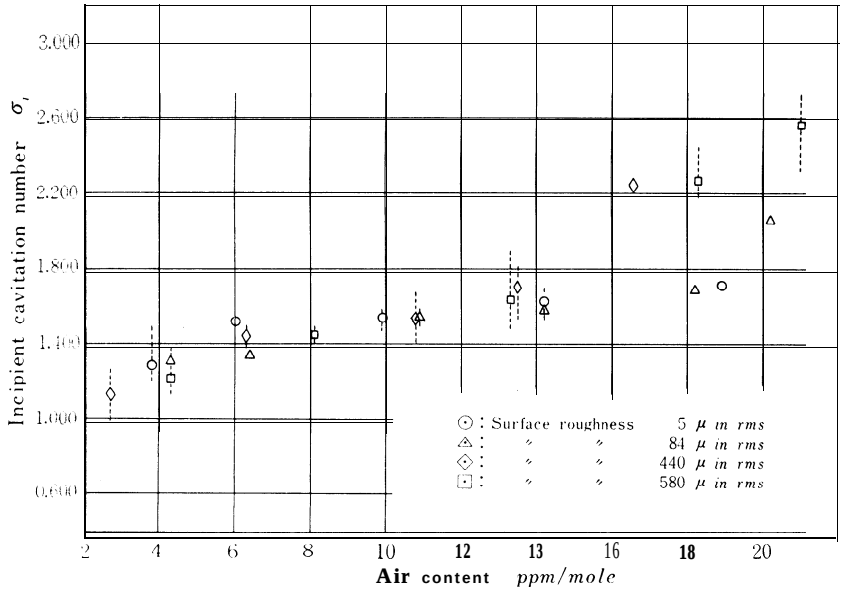

Fig. 43. Incipient cavitation number vs air content for blunt nose (V_0=43.52 ft/sec).

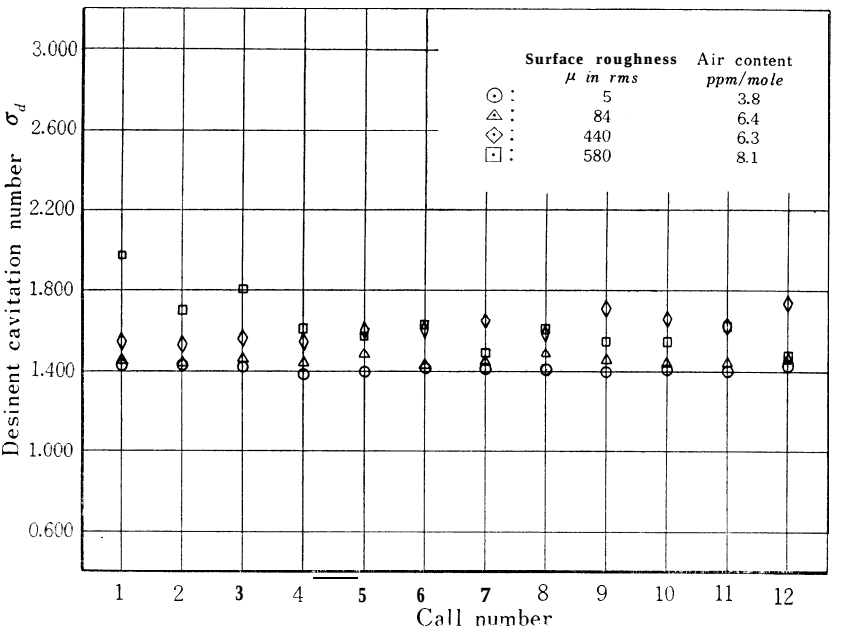

Fig. 44. Desinent cavitation number for blunt nose (V_0– 32.42 ft/sec).

are for hemispherical noses and Figs. 44 and 45 are for blunt noses. The scale of cavitation number for hemispherical noses is two and one-half times, and that for blunt noses is ten times as large as that for 1.5 caliber ogive noses.

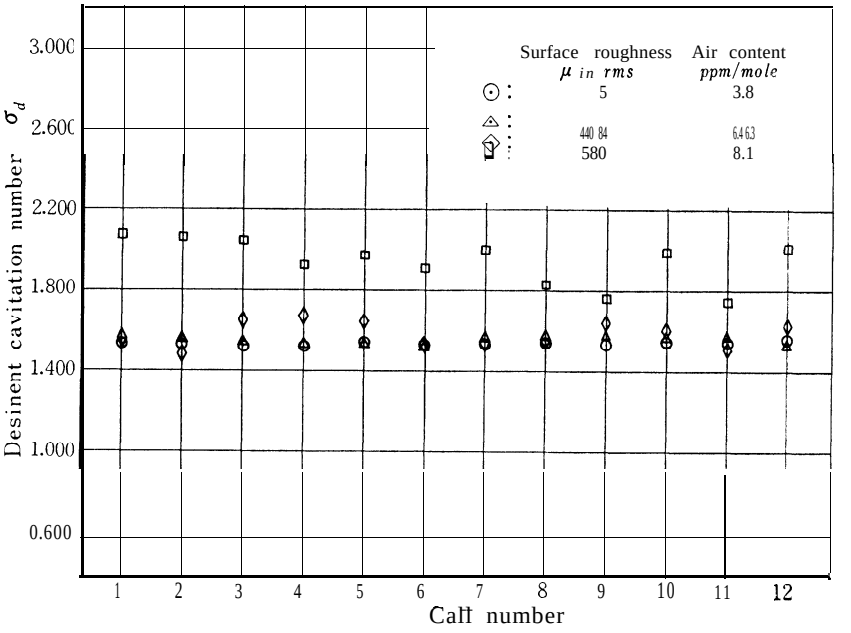

Fig. 45. Desinent cavitation number for blunt nose (V_0 = 43.52 ft/sec).

Discussions

1. Correlations with other data

To see how this data compares with other investigators' results, the data obtained for the caliber 1.5 ogive smooth nose and the hemispherical smooth nose are compared to the data obtained by California Institute of Technology and Ordnanse Research Laboratory of Pennsylvania State University.[20] From CIT and ORL data, the desinent cavitation numbers for the 1/2 inch hemispherical nose at a dissolved air content of 7.7 ppm are 0.54 and 0.59 for velocities of 32 and 44 feet per second respectively. Comparing these values to Figs. 34 and 36, it can be concluded that the correlation is good. Although the data of Figs. 28 and 30 for the caliber 1.5 ogive nose is somewhat higher than the CIT and ORL data, the correlation is fairly close. The same reference has shown that the desinent cavitation number increased with the increase of free stream velocity. Comparison of Fig. 32 to 31, Fig.

38 to 39 and Fig. 44 to 45 show the same trend. Therefore, the differences in desinent cavitation numbers between for high and for low free stream velocity could be considered as the velocity effect on cavitation number.

2. Effects of surface roughness

As shown Figs. on 33 and 38, the desinent cavitation number becomes larger as the surface roughness value becomes larger. In general, the differences in the desinent cavitation number between smooth noses and sand blasted noses are small. Sometimes, the desinent cavitation number for a smooth nose is larger than that for a sand blasted nose, as Fig. 33. It shows the same trend as Kermeen's result.[15] For steel shot blasted noses, desinent cavitation numbers become very large in the cases of caliber 1 and 1.5 ogive noses, indicating that there are significant pressure reductions at rough points. Close observations of the onsets of cavitation for each nose clearly show the fact. For examples, sketches in Fig. 46 are observed patterns of cavitation on caliber 1.5 ogive noses. The onset of cavitation on a smoother nose

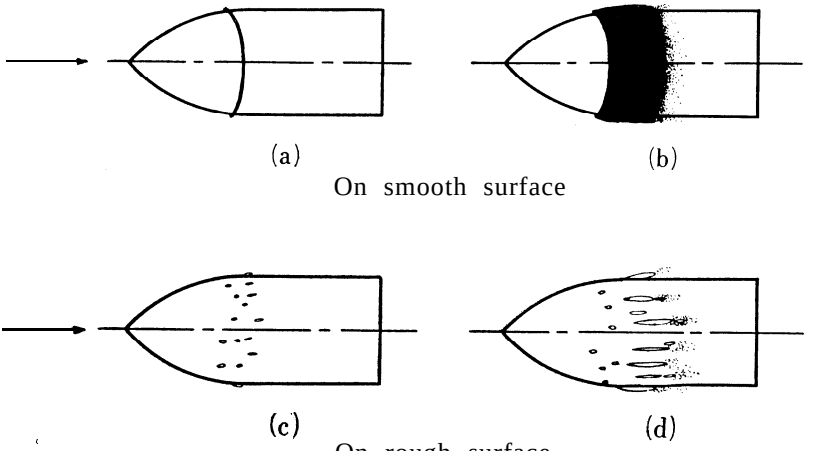

Fig. 46. Cavitation on caliber 1.5 ogive nose.

(smooth nose or sand blasted nose) appears as a fine ring on the nose as the sketch (a). As the static pressure decreases, it grows to cavitation as (b). Sketch (c) shows the pattern of the onset of cavitation on a rough nose (steel shot blasted). The onset occurs as small bubbles attached on the surface at rough points. They grow to cavitation as (d). It could be said from above observations that the height of roughness on a sand blasted nose is not enough to cause local pressure reduction.

The pattern of cavitation onset on the blunt nose does not change as the surface roughness changes. It occurs as the sketch (a) of Fig. 47. It grows to cavitation as (b). Only difference observed between

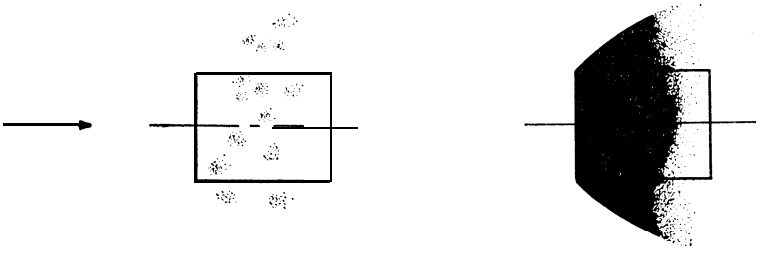

Fig. 47. Cavitation on blunt nose.

on smooth nose and on rough nose is that the bubble radius on a smooth nose seems finer than that on a rough nose. For this nose, the surface roughness does not have systematical effects on the onset of cavitation. Considering the effect of air content, desinent cavitation numbers for different surface roughnesses seem to have values of the same order.

3. Cavitation hysteresis

For almost all cases, so-called cavitation hysteresis is observed. Obtaining inception pressure, sometimes a significant low pressure is reached before cavitation appears. Cavitation suddenly begins at the low pressure and forms a fully developed cavitation. For an example, cavitation hysteresis for an hemisphere nose is seen on Fig. 48. From the figure, it seems to have a sensible relation with air content.

4. Effect of air content

The test showed the existence of a close relation between the cavitation number and the air content of water. In general, the desinent cavitation number and the incipient cavitation number increase as the air content of water increases. The trend is larger for hemispherical noses than for caliber 1.5 ogive noses and it becomes largest for the blunt noses as shown on Figs. 31, 37 and 43. Desinent cavitation numbers for rough noses of caliber 1.5 ogive noses (excepting the data for low velocities because of the difficulty of observation) and of hemispherical noses were not affected much by air content as shown on Figs. 30, 34 and 36. Incipient cavitation numbers for rough noses were affected by air content much more than desinent cavitation numbers as on Figs. 35 and 37. This is probably caused by the fact that the

gaseous cavitation always occurred for rough noses when the air content was high, while it was not so likely to occur when air content was relatively low. The effect of air content on the desinent and incipient

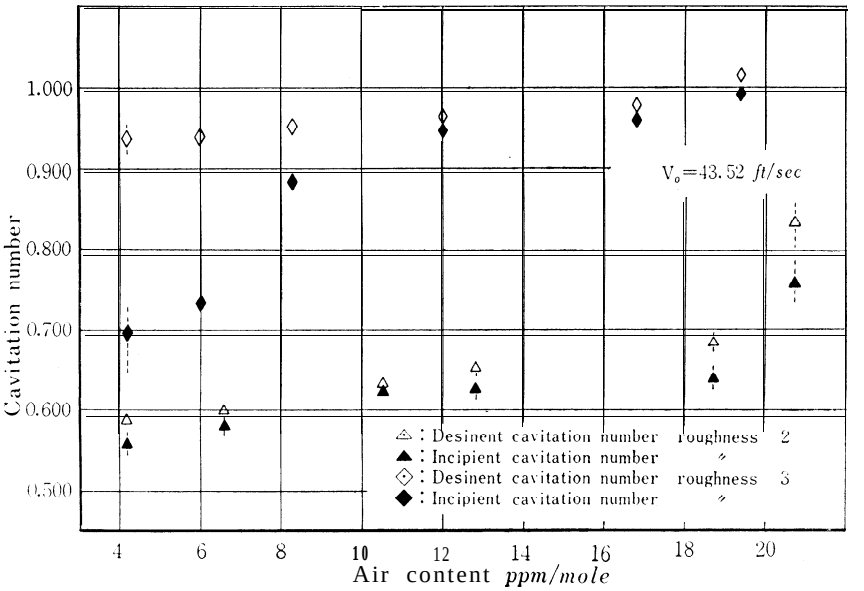

Fig. 48. Cavitation hysteresis on hemispherical nose.

cavitation numbers for smoother noses seemed about the same. For smoother noses, the gaseous cavitation was not observed for either desinent or incipient conditions.

Conclusions

The major conclusions of the test are summarized as follows.

1. The desinent cavitation number increases as the surface roughness increases for caliber 1.5 ogive noses and hemispherical noses. The trend is not clear for blunt noses.

2. For caliber 1.5 ogive noses and hemispherical noses, the change in the desinent cavitation number becomes larger as the surface roughness becomes larger. The change between smooth noses and sand blasted noses is small.

3. Cavitation hysteresis is observed for almost all cases. The difference between the desinent cavitation number and the incipient cavitation number becomes larger as the air content decreases.

4. The air content has an effect on the cavitation number.

5. Both desinent and incipient cavitation numbers become larger as the air content becomes higher.

SUMMARY

Because of undesirable effects of cavitation, the design of a cavitation free structure is an important problem in the field of Hydraulic Engineering. The surface of an ordinary hydraulic structure has roughness, scattered randomly or isolated. Only few investigations have been done on the effects of surface roughness on cavitation. Therefore, " the effects of randomly distributed surface roughness on cavitation " is investigated in this paper.

For the experimental investigation of the problem, a circulating type 6 inch water tunnel is designed and constructed at the Hydraulic Laboratory of Civil Engineering Department, the Pennsylvania State University, U.S.A. The test section of the tunnel has a cylindrical cross section with an inside diameter of 6 inches and a length of 24 inches. An axial flow propeller pump (9 inches in diameter), driven by a two speed motor, is installed for the circulation of water. The velocities in the test section corresponding to high and low motor speed are 43.52 and 32.42 feet per second. The static pressure in the test section is controlled by the pressure control system and a vacuum pump. The range of the static pressure is from 2 psia to 85 psia.

The models employed in the test are three families of 3/4 inch diameter stainless steel noses having 1.5 caliver ogive, hemispherical and blunt profiles. Each family consists of four noses having different surface roughness. The first one is polished with hand, the second is roughened with sand blasting and the third and forth are roughened with steel shot. The surface roughness ranges from 2.8 to 580 μ in rms.

The test is conducted in the 6 inch water tunnel, and consists of finding the desinent cavitation number and the incipient cavitation number under different conditions. The air content of water is measured for each test run using a Van Slyke equipment.

The test results show that, in general, the cavitation number for the onset condition increases significantly as the surface roughness increases. In addition, it is seen from the results that there is a close correlation between the air content of water and the onset of cavitation. In general, the cavitation number for the onset condition increases as the air content of water increases.

ACKNOWLEDGEMENT

The author deeply appreciates the guidance and constructive criticisms of Dr. Kunimi Tanabe of Kyushu University. Appreciation is also expressed to Professors Samuel Shulits, George F. Wislicenus and

August F. Lehman of the Pennsylvania State University, U.S.A. In addition, the Pennsylvania State University's Ordnance Research Laboratory and civil Engineering Department are thanked for the test equipment and housing of the equipment.

REFERENCES

1) Calehuff, G. L. and Wislicenus, G. F. 1956, ORL investigation of scale effects on hydrofoil cavitation. Ordnance Research Laboratory TM 19. 4211-03, the Pennsylvania State University.
2) Colgate, D. 1959. Cavitation damage of roughened concrete surfaces. Proceedings of ASCE, Vol. 11, No. HY 11.
3) Degarabedian, P. 1953. The rate of growth of vapor bubbles in superheated water. Journal of Applied Mechanics, Vol. 20.
4) Fisher, J. C. 1948. The fracture of liquids. Journal of Applied Physics, Vol. 19.
5) Fox, F. E. and Herzfeld, K. F. 1954. Gas bubbles with organic skin as cavitation nuclei. Journal of the Acoustical Society of America, Vol. 29.
6) Frenkel, J. 1946. Kinetic theory of liquids. Oxford, New York.
7) Gilmore, F. R. and Plesset, M. S. 1950. Scaling laws for incipient cavitation noise. Hydrodynamics Laboratory, California Institute of Technology, Report 26-l.
8) Harrold, J. C. 1945. Cavitation in hydraulic structures-a symposium, experiences of the Corps of Engineers, Proceeding of ASCE, Vol. 71.
9) Harvey, E. N., McElroy, W. D. and Whiteley, A. H. 1947. On cavity formation in water. Journal of Applied Physics, Vol. 18.
10) Hickox, G. H. 1945. Cavitation in hydraulic structures-a symposium, experiences of the Tennessee Valley Authority. Proceeding of ASCE, Vol. 71.
11) Holl, J. W. 1958. The effect of surface irregularities on incipient cavitation. Ph. D. Dissertation, Department of Mechanical Engineering, the Pennsylvania State University.
12) Holl, J. W. 1960. An effect of air content on the occurrence of cavitation. Transactions of the ASME, Paper No. 60-Hyd-8.
13) Holl, J. W. and Wislicenus, G. F. 1960. Scale effects on cavitation. Ordnance Research Laboratory, the Pennsylvania State University.
14) Jones, I. R. 1959. The measurement of the pressure due to the collapse of cavities in liquids. Doctoral dissertation, University of Wales, Aberystwyth, England.
15) Kermeen, R. M. 1952. Some observations of cavitation on hemispherical head models. California Institute of Technology Hydrodynamics Laboratory Report E-53. 1.
16) Kyushu Denryoku Kabushiki-Kaisha, Dobokubu. 1957. Arch dam, the planning and the execution of Kamishiiba-dam. Maruzen.
17) Milene-Thomson, L. M. 1938. Theoretical hydrodynamics. Macmillan.
18) ORL External Report. 1948. Water tunnel working section flow studies. The Pennsylvania State University, Ser. No. NOrd 7958-97.

19) ORL External Report. 1949. Water tunnel diffuser flow sudies, Part II—experimental research. The Pennsylvania State University, Ser. No. NOrd 7958-143.
20) Parkin, B. R. and Holl, J. W. 1953. Incipient cavitation scaling experiments for hemispherical and 1.5-caliber ogive-nosed bodies. ORL Report, the Pennsylvania State University, Ser. No. Nord 7958264.
21) Peters, H. and Rightmire, B. G. 1938. Cavitation study by vibratory method. Proceedings, Fifth International Cong. for Applied Mechanics.
22) Plesset, M. S. and Zwick, S. A. 1952. A nonsteady heat diffusion problem with spherical symmetry. Journal of Applied Physics, Vol. 23.
23) Plesset, M. S. and Ellis, A. T. 1955. On the mechanism of cavitation damage. Transactions of the ASME, Vol. 77, No. 7.
24) Ross, D., Robertson, J. M. and Power, R. B. 1948. Hydrodynamic design of the 48-inch Water Tunnel at the Pennsylvania State College. Transactions, Soc. Naval Architects & Marine Engineers, Vol. 5b.
25) Streeter, V. L. 1961. Handbook of fluid dynamics. McGraw-Hill Book Company*
26) Tanabe, K., Kaku, K. and Hiraoka, H. 1963. On the study of cavitation. on hydraulic structure surfaces. Transactions of the Agricultural Engineering Society, Japan, No. 6.
27) Waker, G. K. 1957. Rotational flow over a surface protrusion. Master of Science Dissertation, Department of Aeronautical Engineering, the Pennsylvania State University.